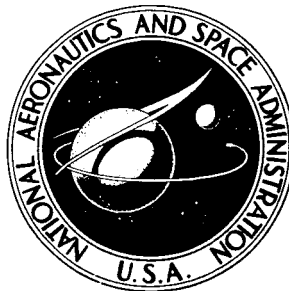


NASA TECHNICAL NOTE



NASA TN D-7498

NASA TN D-7498

**CASE FILE
COPY**

**THEORETICAL AND EXPERIMENTAL
INVESTIGATION OF THE PERFORMANCE
OF A FAN-IN-WING VTOL CONFIGURATION**

*by Harry H. Heyson
Langley Research Center
Hampton, Va. 23665*

NATIONAL AERONAUTICS AND SPACE ADMINISTRATION • WASHINGTON, D. C. • DECEMBER 1973

1. Report No. NASA TN D-7498	2. Government Accession No.	3. Recipient's Catalog No.	
4. Title and Subtitle THEORETICAL AND EXPERIMENTAL INVESTIGATION OF THE PERFORMANCE OF A FAN-IN-WING VTOL CONFIGURATION		5. Report Date December 1973	
		6. Performing Organization Code	
7. Author(s) Harry H. Heyson		8. Performing Organization Report No. L-9219	
		10. Work Unit No. 760-61-02-01	
9. Performing Organization Name and Address NASA Langley Research Center Hampton, Va. 23665		11. Contract or Grant No.	
		13. Type of Report and Period Covered Technical Note	
12. Sponsoring Agency Name and Address National Aeronautics and Space Administration Washington, D.C. 20546		14. Sponsoring Agency Code	
		15. Supplementary Notes	
16. Abstract <p>The incompressible-flow momentum theory of NASA TN D-814 is extended to the case of lifting fans. The resulting theory includes many of the known experimentally determined characteristics of fan-in-wing aircraft. These characteristics include the negligible effect of forward speed on fan thrust, the large momentum drag, and the generally inefficient performance throughout the transition speed range. Although mutual interference between the fans and the wing was totally neglected, the theory is confirmed by experimental results for the configuration tested. Examination of the results of an investigation of wall interference leads to the conclusion that the large "fan-induced" lift reported in many earlier investigations was largely the result of neglecting wall interference in the reduction of wind-tunnel data.</p>			
17. Key Words (Suggested by Author(s)) Fan-in-wing VTOL Momentum theory Mutual interference Flow fields Wind-tunnel wall effects		18. Distribution Statement Unclassified - Unlimited	
19. Security Classif. (of this report) Unclassified	20. Security Classif. (of this page) Unclassified	21. No. of Pages 73	22. Price* Domestic, \$3.50 Foreign, \$6.00

THEORETICAL AND EXPERIMENTAL INVESTIGATION OF THE PERFORMANCE OF A FAN-IN-WING VTOL CONFIGURATION

By Harry H. Heyson
Langley Research Center

SUMMARY

The incompressible-flow momentum theory of NASA TN D-814 is extended to the case of lifting fans. The resulting theory includes many of the known experimentally determined characteristics of fan-in-wing aircraft. These characteristics include the negligible effect of forward speed on fan thrust, the large momentum drag, and the generally inefficient performance throughout the transition speed range. Although mutual interference between the fans and the wing was totally neglected, the theory is confirmed by experimental results for the configuration tested. Examination of the results of an investigation of wall interference leads to the conclusion that the large "fan-induced" lift reported in many earlier investigations was largely the result of neglecting wall interference in the reduction of wind-tunnel data.

INTRODUCTION

Efforts to design a viable aircraft capable of vertical flight and, at the same time, capable of efficient high-speed flight have produced a wide array of configurations. Of these configurations, lifting-fan types have been among the more prominent and the more persistently pursued. One flight vehicle (the XV-5) has been built and the possibility of commercial-service configurations is presently being studied. (See refs. 1 and 2.)

Despite the interest in lift-fan configurations, there is little in the way of an adequate theory to guide their design. Most of the design information has been obtained in a purely empirical manner from wind-tunnel tests. (See, for example, refs. 3 to 14.) Even these wind-tunnel tests are less than completely adequate. For example, such a primary quantity as the power supplied to the fans is seldom measured or presented. Furthermore, considerable disagreement exists in these studies as to the amount of "fan-induced" lift which will be obtained in the transition speed range. (Compare, for example, refs. 3 to 10 with refs. 13 and 14.)

The present investigation stems directly from a study of wind-tunnel wall interference (ref. 15) which utilized a simple fan-in-wing model. In the course of correcting the

data of that investigation, it was necessary to develop a theoretical means of predicting the effect of wall-induced distortions of the flow in the region of the model. The theory derived for this purpose proved capable of predicting many other facets of the observed model performance; therefore, it is presented independently in the present paper as a starting point for the development of a viable theory for fan-supported aircraft.

The present theory is a direct extension of the generalized V/STOL momentum theory originally presented in reference 16. In its original form, this theory is equivalent to rotary-wing momentum theory (ref. 17); has found application to unusual configurations (ref. 18); and has formed the basis for further experimentally confirmed investigations by others (ref. 19). The one essential feature to the present development is the accommodation of one special restraint in the case of the lifting fan, namely, that the initial direction of the wake is constrained to be along the effective axis of the fan. The consequences of this feature are far reaching and result in an induced performance which differs notably from that of most other lifting systems.

Particular attention is given to the calculation of the required fan power. This feature is of paramount significance since most of the wind-tunnel investigations provide no indication of the actual power required during transition even though the installed power in some of the models was exceptionally large. In addition, the equivalent lift-drag ratio is derived; as a result, a rational rapid comparison with other configurations at equal speeds is possible.

The present treatment contains a number of gross oversimplifications. For example, the flow is assumed to be incompressible even though the pressure ratio of proposed fans may be as great as 1.3. In addition, in the fan-in-wing case, it is assumed that there is no mutual interference between the fans and the wing. (An appendix provides a qualitative discussion of this interference.) Nevertheless, the experimental results presented herein indicate reasonably close agreement with the theory for this model.

The present theoretical and experimental study does not indicate the large fan-induced lifts which are a notable feature of many previous investigations. (See, in particular, ref. 3.) Reference 15 shows clearly that these earlier indications of large favorable interference during transition are largely caused by the omission of corrections for wall interference in reducing the wind-tunnel data. A few results from reference 15 are included to illustrate the magnitude of the wall-interference effects.

SYMBOLS

C_D drag coefficient based on wing area and free-stream dynamic pressure,
 D/qS_W

$C_{D,j}$	drag coefficient based on fan area and fan-exit dynamic pressure, $D/q_j S_F$
C_L	lift coefficient based on wing area and free-stream dynamic pressure, $L/q S_W$
$C_{L,j}$	lift coefficient based on fan area and fan-exit dynamic pressure, $L/q_j S_F$
c	local chord
D	external induced, or momentum, drag force parallel to X-axis, positive rearward. (In the experimental data, D is taken as the total drag less the drag at $\alpha = 0^\circ$.)
D_e	drag equivalent to total power requirement
D_{se}	drag equivalent to shaft power requirement
\vec{F}	force vector generated by an aerodynamic device
L	lift, force parallel to Z-axis, positive upward
n	ratio of induced velocities in far wake to those at aerodynamic device
P_s	shaft power
$P_{s,h}$	shaft power due to lift, in hovering, $-Lw_h$
$P_{s,S}$	shaft power in static thrust, $T_S V_j$. (See eq. (31) for the relationship between $P_{s,h}$ and $P_{s,S}$.)
P_t	total power
q	free-stream dynamic pressure, $\frac{1}{2} \rho V^2$
q_j	fan-exit dynamic pressure, $\frac{1}{2} \rho V_j^2$
R	local body radius
S	area

T_S	static thrust
u_0	mean longitudinal induced velocity at lifting device, positive rearward along X-axis
V	forward velocity
V_j	fan-exit velocity in static thrust, $\sqrt{T_S/\rho S_F}$
V_R	resultant velocity at aerodynamic device, magnitude of \vec{V}_R , always positive
\vec{V}_R	vectorial resultant velocity at aerodynamic device
w_0	mean vertical induced velocity at aerodynamic device, positive upward along Z-axis
w_h	value of w_0 when $V = 0$ and $D = 0$, positive upward along Z-axis
X, Y, Z	Cartesian coordinate system centered in aerodynamic device, X-axis is positive rearward, Z-axis is positive upward, Y-axis is positive laterally to form a right-handed system. Observe that the positive direction of forces and velocities generally agree with the positive direction of the axis along which they lie. X and Z in tables I and II are defined in sketch accompanying the table.
α	angle of attack, positive nose-up from negative X-axis, radians in equations, degrees in figures
ΔD	a small change in drag
ΔL	a small change in lift
ΔV	a small change in forward velocity
$\Delta \alpha$	a small change in angle of attack, radians
θ_n	net downwash angle, $90^\circ - \chi$, positive downward, deg
ρ	mass density of air

χ wake skew angle, angle measured positive rearward from the negative Z-axis to center of the wake, deg (Note that this definition differs from that used in the appendix.)

Subscripts:

F fans

M measured

t total

W wing

THEORY

Basic Equations

Generalized momentum quartic. - It is assumed that the fluid influenced by any lifting device can be represented by a uniformly affected flow passing through a representative area S_F . (See fig. 1.) In axial flight, it is obvious that S_F is identical with the fan area. In cross flow, the representative area is assumed to be the same area S_F . This assumption follows Glauert's treatment of the helicopter rotor (ref. 20), which, in turn, was based upon Prandtl's observations on the affected area for a wing (ref. 21). Although Glauert's hypothesis was purely empirical, it will be observed that this assumption leads directly to the identical result that is obtained by simple vortex theory (ref. 17) for a rotor. Thus, from figure 1, since force is equal to the timewise rate of change of momentum

$$L = \rho S_F V_R (-nw_0) \quad (1)$$

$$D = \rho S_F V_R (-nu_0) \quad (2)$$

where n is the ratio of the induced velocities in the far wake to the induced velocities at the lifting system. For a fully expanded efflux from a ducted fan in axial flight, n should be equal to 1. Except for axial flight, there is no assurance that n is indeed equal to 1; however, in many cases the results may be expressed in terms of ratios in which n does not appear.

It suffices to divide equation (2) by equation (1) in order to show that the induced velocity components are in the same proportion as the force components; that is,

$$\frac{D}{L} = \frac{u_0}{w_0} \quad (3)$$

Solve equation (1) for w_0 , and multiply both sides of the resulting equation by w_0 to obtain

$$w_0^2 = \frac{L}{n\rho S_F \frac{V_R}{-w_0}} \quad (4)$$

Evaluation of equation (4) requires V_R which may be obtained from the velocity vectors of figure 1 as

$$V_R = \sqrt{(V + u_0)^2 + (-w_0)^2} \quad (5)$$

Divide both sides of equation (5) by $-w_0$ and use equation (3) to obtain

$$\frac{V_R}{-w_0} = \sqrt{1 + \left(\frac{V}{w_0} + \frac{D}{L}\right)^2} \quad (6)$$

At this point, it is convenient to introduce a reference velocity w_h . This reference velocity is defined as that induced velocity which would be obtained in hovering ($V = 0$), with zero drag ($D = 0$), and with the same lift L , and effective area S_F . Under these conditions, equation (6) reduces to

$$V_R = -w_h \quad (7)$$

and equation (4) becomes

$$w_h^2 = \frac{L}{n\rho S_F} \quad (8)$$

In taking the square root of both sides of equation (8), observe that in the present coordinate system, a positive lift requires a negative vertical induced velocity; thus,

$$w_h = -\sqrt{\frac{L}{n\rho S_F}} \quad (9)$$

Observe that the reference velocity w_h does not even need to exist in a real world; it may be completely fictitious. The same relationship, for example, can be applied to a simple wing which is incapable of hovering. In the present case, it does have a real physical meaning which will be developed in later sections of this paper.

Division of equation (4) by equation (8) yields

$$\left(\frac{w_0}{w_h}\right)^2 = \frac{-w_0}{V_R} \quad (10)$$

Finally, substitute equation (6) into equation (10) and square both sides to obtain the generalized momentum quartic

$$\left(\frac{w_0}{w_h}\right)^4 = \frac{1}{1 + \left(\frac{V}{w_0} + \frac{D}{L}\right)^2} \quad (11)$$

Reference 16 demonstrates that equation (11) is identical (except for notation) with the expressions for helicopter rotors developed by Wald (ref. 22) and by Coleman, Feingold, and Stempin (ref. 23).

The wake skew angle. - The wake skew angle χ of the resultant flow at the fan is the complement of the net downwash angle θ_n . It may be obtained from inspection of the flow vectors in figure 1 as

$$\tan \chi = -\left(\frac{V}{w_0} + \frac{D}{L}\right) \quad (12)$$

An alternate form may be obtained by substituting equation (12) into equation (11) and simplifying to yield

$$\cos \chi = \left(\frac{w_0}{w_h} \right)^2 \quad (13)$$

Note that χ is defined with respect to the axes defining lift and drag.

Reference 16 develops a chart of the foregoing generalized equations. A simplified version of this chart is presented in figure 2; discussion of figure 2 will be delayed to a later point in this paper.

Shaft power.- The shaft power required by any aerodynamic device is merely the scalar (or dot) product of the force and velocity vectors; that is, with the present sign convention

$$P_s = -\vec{F} \cdot \vec{V}_R \quad (14)$$

or, upon expansion into Cartesian coordinates

$$P_s = -D(V + u_0) - Lw_0 \quad (15)$$

In hovering with zero drag, equation (15) reduces to

$$P_{s,h} = -Lw_h \quad (16)$$

Divide equation (15) by equation (16), and substitute for u_0/w_0 from equation (3) to obtain, after some simplification,

$$\frac{P_s}{P_{s,h}} = \frac{D}{L} \frac{V}{w_h} + \left[1 + \left(\frac{D}{L} \right)^2 \right] \frac{w_0}{w_h} \quad (17)$$

The first term on the right-hand side of equation (17) represents the power associated with an external induced (or momentum) drag force. Since V/w_h is intrinsically negative, the entire term is negative for a positive drag; that is, energy extracted from the air reduces the shaft power requirement. Obviously, energy must be supplied elsewhere, either from propulsion engines or from loss of altitude, in order to maintain steady flight. If D/L is sufficiently large, the total shaft power requirement may be zero or even negative. Obviously, this condition applies to an autogyro rotor. For negative drag

or forward propulsive thrust, the first term on the right-hand side of equation (17) is always positive; this term then represents the power required to overcome an external drag (such as parasite drag) elsewhere in the system.

Since both w_0/w_h and $\left[1 + \left(\frac{D}{L}\right)^2\right]$ are always positive, the final term of equation (17) is always positive. The induced power required to produce lift in the absence of drag is given by w_0/w_h . The term $\left[1 + \left(\frac{D}{L}\right)^2\right]$ is an expansion factor representing the obvious fact that the resultant force is greater than just the lift when a drag force is present. Indeed, both the resultant force and the resultant induced velocity are increased over L and w_0 by a factor of $\sqrt{1 + \left(\frac{D}{L}\right)^2}$.

The Isolated Lifting Fan

General considerations. - The distinctive feature of the lifting fan is the directed nature of its efflux. If there are no deflection vanes in the exit, if the duct has any reasonable depth, and if the disk loading is reasonably high, the exit flow from the fan will be directed along the axis of the exit. This assumption is verified by the calculations made in the course of preparing reference 15. Furthermore, it is the inherent physical reason behind calculations of fan "ram drag," such as those presented in reference 3. Exit vanes, if provided, will turn the flow from this direction; however, the resulting system can be viewed as an equivalent vaneless system with an altered angle of attack and perhaps (if the vane deflection throttles the exit) with an altered fan area. Obviously, exit vanes will increase the required power due to their parasite drag in the high-velocity fan efflux.

Parameters used in analysis. - The present analysis proceeds in terms of the parameters used in the preceding sections of this paper and in reference 16; however, these parameters differ somewhat from those customarily used in presenting lifting-fan performance. The more generally used parameters are V/V_j (where V_j is the absolute velocity of the fan efflux in hovering) and T_S (where the static thrust is defined as the resultant force in hovering). Since the conversion between the different forms is relatively simple, important results will be restated in terms of T_S and V/V_j .

To accomplish the conversion of parameters, observe that since force is the time-wise rate of change of momentum (fig. 3) and n is assumed to be 1,

$$T_S = \rho S_F V_j^2 \tag{18a}$$

and

$$L = T_S \cos \alpha \quad (18b)$$

At this point, equation (18b) is presented for convenience in some of the subsequent equations. This expression requires proof. The proof will be provided in a later section.

Substitute equations (18) into equation (9) and solve for w_h to obtain

$$w_h = -V_j \sqrt{\cos \alpha} \quad (18c)$$

Induced velocity ratio.- Under the aforementioned assumptions, the fan (fig. 3) accepts the incoming fluid at a velocity V and turns it so that the net longitudinal velocity at the exit is $-V_R \sin \alpha$. Thus, the longitudinal induced velocity at the fan is

$$u_0 = -(V + V_R \sin \alpha) \quad (19)$$

Observe that at zero angle of attack, u_0 is simply equal and opposite to V . Substitute equation (19) into equation (5) and solve for $-w_0/V_R$

$$\frac{-w_0}{V_R} = \cos \alpha \quad (20)$$

and then substitute equation (20) into equation (10) to obtain

$$\frac{w_0}{w_h} = \sqrt{\cos \alpha} \quad (21)$$

As might have been foreseen, a comparison of equations (13) and (21) indicates that for the lifting fan, the wake skew angle χ has been replaced by α (or, more properly, by $-\alpha$). Observe that at constant angle of attack, the vertical induced velocity of the fan is totally unaltered by forward velocity. This result is a consequence of the large horizontal induced velocity and is in stark contrast to most other lifting systems where, since D/L is small, figure 2 shows that the vertical induced velocity decreases rapidly with forward speed. Indeed, the slowly varying nature of the function $\sqrt{\cos \alpha}$ demonstrates that extreme angles of attack would be required to produce any significant reduction in the vertical induced velocity of the lifting fan.

External drag.- The external drag of the lifting fan is obtained by substituting equations (19), (20), and (21) into equation (2) and simplifying to yield

$$D = \frac{-n\rho S_F w_h}{\sqrt{\cos \alpha}} \left(V - w_h \sqrt{\cos \alpha} \tan \alpha \right) \quad (22)$$

At zero angle of attack, equation (22) reduces to simply $D = -n\rho S_F w_h V$ and is precisely the result that would be written from elementary considerations of the inlet momentum drag. (Assume that $n = 1$; then $-\rho S_F w_h$ is the mass-flow rate, and V is the change in velocity.) The additional terms in equation (22) represent the propulsive thrust and the changes in w_0 which occur as a result of changes in angle of attack. Equation (22) shows that D is a linear function of V , the slope and the value at $V = 0$ being determined by α and w_h . This result is in contrast to the behavior of most systems where the drag generally is proportional to V^2 .

The ratio of the external drag to the static thrust is found by substituting equations (18) into equation (22) to yield

$$\frac{D}{T_S} = \frac{V}{V_j} + \sin \alpha \quad (23)$$

The ratio of external drag to static thrust has additional significance in that it is proportional to a drag coefficient based on fan parameters. This effect may be seen from the definitions of $C_{D,j}$ and T_S since

$$C_{D,j} = \frac{D}{\frac{\rho}{2} V_j^2 S_F} = \frac{2D}{\rho S_F V_j^2} = 2 \frac{D}{T_S} \quad (24)$$

Lift.- The fan lift is obtained by substituting equations (20) and (21) into equation (1) to obtain

$$L = n\rho S_F w_h^2 \quad (25)$$

which, together with equation (21), proves that the lift is unaltered by forward velocity V . Since the lift is unaltered, simple geometric considerations lead immediately to the conclusion that

$$\frac{L}{T_S} = \cos \alpha \quad (26)$$

thus, the relationship given earlier in equation (18b) has been proved.

Observe that, in consequence of equation (26), the lift is totally independent of forward speed; indeed, at $\alpha = 0^\circ$, it is always equal to the static thrust. This tendency has been confirmed repeatedly by momentum-rake measurements of thrust in the wind tunnel. Indeed, figure 6 of reference 10 shows that, in the typical fan lift system, only 10 to 15 percent of the thrust is lost up to $V/V_j \approx 0.6$.

The ratio L/T_S is also proportional to a coefficient based on the fan parameters. In this case

$$C_{L,j} = \frac{L}{\frac{\rho}{2} V_j^2 S_F} = \frac{2L}{\rho S_F V_j^2} = 2 \frac{L}{T_S} \quad (27)$$

Relationship to other lifting systems. - At this point, it is profitable to return to figure 2 in order to examine, in general terms, the performance of an isolated lifting fan. This performance differs significantly from the performance of most other lifting systems.

Most VTOL systems (for example, tilt wings and rotors) combine the capability of producing propulsive thrust simultaneously with lift. Thus, the overall induced drag-lift ratio of these systems does not differ markedly from zero throughout their speed range. In the context of figure 2, such systems approximately follow the curve marked $D/L = 0$. As a consequence, the induced-velocity ratio w_0/w_h decreases rapidly and the wake skew angle increases rapidly as the forward speed increases. The result is that the induced power required to produce lift (eq. (17)) decreases rapidly with forward speed.

The isolated lifting fan has totally different characteristics than the aforementioned systems. In this case, the induced-velocity ratio remains constant at $w_0/w_h = \sqrt{\cos \alpha}$ as the forward speed increases. As noted earlier, there is a direct correspondence between α and χ for the lifting fan; thus, the χ -scale of figure 2 may be interpreted as indicating the absolute value of α . Consequently, the lifting fan at constant angle of attack follows a path parallel to the abscissa directly across figure 2 as the forward speed increases. As a result, the induced power required to produce lift does not decrease with forward speed, and the fan is substantially less efficient as a lift producer than most other VTOL configurations.

The value of w_0/w_h as a function of forward speed can be reduced by a suitably programmed reduction in α with forward speed (as in the X-22 aircraft). Very large

negative angles of attack (as measured from the vertical axis of the fan) are required; for example, an angle of attack of -36° reduces w_0/w_h by about 10 percent and an angle of attack of -50° reduces w_0/w_h by about 20 percent. Such large negative fan angles of attack are not appropriate to configurations in which the fans are fixed with respect to the wings. These considerations indicate that if, for reasons other than aerodynamic efficiency, it is desirable to use lifting fans, more efficient configurations will result if it is possible to rotate the fans independently of the wing.

External drag-lift ratio.- The external drag-lift ratio is obtained by dividing equation (22) by equation (25) to yield

$$\frac{D}{L} = \frac{-V/w_h}{\sqrt{\cos \alpha}} + \tan \alpha \quad (28)$$

or, in terms of V/V_j

$$\frac{D}{L} = \frac{V/V_j}{\cos \alpha} + \tan \alpha \quad (29)$$

It is obvious from equations (28) and (29) that the external performance of the lifting fan becomes poorer (D/L becomes greater) as the forward velocity increases.

Shaft power.- The shaft power is obtained by substituting equations (21) and (28) into equation (17) and noting that the shaft power in hovering is $P_{S,h} = -Lw_h$

$$\frac{P_S}{P_{S,h}} = \frac{-V}{w_h} \tan \alpha + \frac{1}{\cos^{3/2} \alpha} \quad (30)$$

In converting equation (30) to an equivalent form in terms of V/V_j and α , it should be noted that $P_{S,h}$ in equation (30) is based on only the lift component of thrust and the vertical component of induced velocity. When recast in terms of V/V_j and α , it is desirable to consider a reference static-thrust power $P_{S,S}$ which is based on T_S and V_j ; thus, by use of equations (18)

$$P_{S,h} = -Lw_h = -T_S \cos \alpha \left(-V_j \sqrt{\cos \alpha} \right) = T_S V_j \cos^{3/2} \alpha = P_{S,S} \cos^{3/2} \alpha \quad (31)$$

Whereupon, by the use of equations (18) and (31), equation (30) becomes

$$\frac{P_s}{P_{s,S}} = 1 + \frac{V}{V_j} \sin \alpha \quad (32)$$

Equation (32) shows that at $\alpha = 0^\circ$, the shaft power is unaffected by forward speed. There is an effect of forward speed only if α is other than zero. The shaft power is reduced if the fan is tipped forward (where at low speeds it may even produce a propulsive thrust) and the shaft power is increased if the fan is tipped rearward (where the fan always produces an external drag).

The shaft power becomes zero when $\alpha = -90^\circ$ and $V/V_j = 1.0$. Under these conditions, however, there is neither lift (eq. (26)) nor drag (eq. (23)), since the fan is not affecting the incoming air at all.

Total power. - The shaft power as given by equations (31) and (32) is not the total power requirement. For most forward velocities, there is also an external drag which must be overcome in order to maintain equilibrium flight. If it is assumed that there is no drag other than the external drag of the fan, and that this drag is overcome by a 100-percent-efficient auxiliary propulsive device, the total power becomes

$$\frac{P_t}{P_{s,h}} = \frac{D}{L} \frac{V}{w_h} + \left[1 + \left(\frac{D}{L} \right)^2 \right] \frac{w_0}{w_h} - \frac{D}{L} \frac{V}{w_h} = \left[1 + \left(\frac{D}{L} \right)^2 \right] \frac{w_0}{w_h} \quad (33)$$

Upon substitution of equations (21) and (28), equation (33) becomes

$$\frac{P_t}{P_{s,h}} = \frac{1 - 2 \frac{V}{w_h} \sin \alpha \sqrt{\cos \alpha} + \left(\frac{V}{w_h} \right)^2 \cos \alpha}{\cos^{3/2} \alpha} \quad (34)$$

where, as before, $P_{s,h} = -Lw_h$. Equations (18) and equation (31) can be used to express equation (34) in terms of V/V_j and $P_{s,S} (= T_S V_j)$ as

$$\frac{P_t}{P_{s,S}} = 1 + 2 \frac{V}{V_j} \sin \alpha + \left(\frac{V}{V_j} \right)^2 \quad (35)$$

from whence it may be seen that the total power requirement increases rapidly with forward speed. Observe that in equation (35) the total power of the isolated fan is less when the fan is tipped forward (possibly producing propulsive thrust) than it is when the fan is at positive α where it always produces an external drag.

Caution must be used in interpreting equations (34) and (35). Observe that in the case of a positive drag, the total power was increased to account for the additional power which must be expended to overcome that drag; on the other hand, in the case of negative drag (or positive propulsive thrust) the total power has been debited by the power expended in producing the propulsive thrust. Under the latter conditions, depending upon the usage, it may be preferable to deal with the shaft power (eqs. (30) and (31)) rather than the total power (eqs. (34) and (35)).

Equivalent lift-drag ratio.- The parameter most directly expressing aircraft efficiency is the lift-drag ratio. For an unpowered aircraft this ratio is the inverse of drag-lift ratio previously derived. A powered-lift aircraft presents a different problem. If the power input to the lifting system is not incorporated into the lift-drag ratio, during conversion to and from wing-borne flight, erroneous results will be obtained for the range penalty associated with a vertical take-off or landing. The problem is averted simply by incorporating a drag equivalent to the power input into the drag term of the lift-drag ratio.

The drag equivalent of the shaft power is obviously

$$D_{se} = \frac{P_s}{V} \quad (36)$$

Use of the expression $P_{s,h} = -Lw_h$ in equation (36) yields

$$\frac{D_{se}}{L} = \frac{-P_s/P_{s,h}}{V/w_h} \quad (37)$$

Substitute equation (30) into equation (37) to obtain

$$\frac{D_{se}}{L} = \tan \alpha - \frac{1}{\frac{V}{w_h} \cos^{3/2} \alpha} \quad (38)$$

or

$$\frac{D_{se}}{L} = \frac{1 + \frac{V}{V_j} \sin \alpha}{\frac{V}{V_j} \cos \alpha} \quad (39)$$

or

$$\frac{D_{se}}{T_S} = \frac{1 + \frac{V}{V_j} \sin \alpha}{V/V_j} \quad (40)$$

The total equivalent drag is obtained by adding the external drag to the equivalent shaft drag; that is, add equations (28) and (38) to obtain

$$\frac{D_e}{L} = - \frac{1 - 2 \frac{V}{w_h} \sin \alpha \sqrt{\cos \alpha} + \left(\frac{V}{w_h}\right)^2 \cos \alpha}{\frac{V}{w_h} \cos^{3/2} \alpha} \quad (41)$$

or equations (23) and (41) to obtain

$$\frac{D_e}{T_S} = \frac{1 + 2 \frac{V}{V_j} \sin \alpha + \left(\frac{V}{V_j}\right)^2}{V/V_j} \quad (42)$$

Finally, invert equation (41) and divide equation (26) by equation (42) to obtain

$$\frac{L}{D_e} = \frac{- \frac{V}{w_h} \cos^{3/2} \alpha}{1 - 2 \frac{V}{w_h} \sin \alpha \sqrt{\cos \alpha} + \left(\frac{V}{w_h}\right)^2 \cos \alpha} \quad (43)$$

$$\frac{L}{D_e} = \frac{\frac{V}{V_j} \cos \alpha}{1 + 2 \frac{V}{V_j} \sin \alpha + \left(\frac{V}{V_j}\right)^2} \quad (44)$$

Equations (43) and (44) indicate that the equivalent lift-drag ratio is zero at $V = 0$. This result is an obvious consequence of the definition of equivalent drag in equation (36); however, it does produce a correct, albeit trivial, result when used in the Breguet

equation – if the fan never starts flying forward, the range is indeed zero. Nonzero values of the equivalent lift-drag ratios are obtained in forward flight; however, these values are extremely small throughout the entire usable transition speed range. For example, at $\alpha = 0^\circ$ and $V/V_j = 0.5$, L/D_e is only 0.4 which is poor by any standard. The very poor efficiency of the lifting fan indicates that the most economical transition to wing-borne flight is likely to be the most rapid possible transition.

Effect of small changes in α and V/V_j on lift and drag. - In many stability analyses is necessary to know the effect of small changes in the operating parameters on the performance of all parts of the aircraft. A similar requirement exists in correcting data for wind-tunnel wall interference (as in ref. 15) where, because of the differing interference over the aircraft, it is necessary to adjust the data to account for effective aerodynamic distortions of the model (ref. 24). For the drag, the simplest approach is to take the partial differentials of equation (23) with respect to α and V/V_j to obtain

$$\frac{\partial \left(\frac{D}{T_S} \right)}{\partial \left(\frac{V}{V_j} \right)} = 1 \quad (45)$$

$$\frac{\partial \left(\frac{D}{T_S} \right)}{\partial \alpha} = \cos \alpha \quad (46)$$

The change in drag due to changes in α and V/V_j is then obtained (by assuming linear small perturbations) as

$$\Delta D = T_S \left(\frac{\Delta V}{V_j} + \Delta \alpha \cos \alpha \right) \quad (47)$$

where $\Delta \alpha$ is in radians.

In a similar manner, by using equation (26)

$$\frac{\partial \left(\frac{L}{T_S} \right)}{\partial \left(\frac{V}{V_j} \right)} = 0 \quad (48)$$

$$\frac{\partial \left(\frac{L}{T_S} \right)}{\partial \alpha} = -\sin \alpha \quad (49)$$

so that

$$\Delta L = -T_S \Delta \alpha \sin \alpha \quad (50)$$

where $\Delta \alpha$ is again in radians.

The Complete Aircraft

Lift and drag. - Before summing the lifts and drags of the components of the aircraft, it is necessary to reduce them to compatible terms. Observe that from equation (18a)

$$T_S = \rho S_F V_j^2 \quad (51)$$

Thus, it follows from the definition of the lift and drag coefficients that

$$\frac{L_W}{T_S} = \frac{C_{L,W} \frac{\rho}{2} V^2 S_W}{\rho S_F V_j^2} = \frac{C_{L,W}}{2} \frac{S_W}{S_F} \left(\frac{V}{V_j} \right)^2 \quad (52)$$

$$\frac{D_W}{T_S} = \frac{C_{D,W} \frac{\rho}{2} V^2 S_W}{\rho S_F V_j^2} = \frac{C_{D,W}}{2} \frac{S_W}{S_F} \left(\frac{V}{V_j} \right)^2 \quad (53)$$

Equations (52) and (53) may be combined with equations (26) and (23) to obtain the total lift and drag of the combination as

$$\frac{L_t}{T_S} = \cos \alpha + \frac{C_{L,W}}{2} \frac{S_W}{S_F} \left(\frac{V}{V_j} \right)^2 \quad (54)$$

$$\frac{D_t}{T_S} = \frac{V}{V_j} + \sin \alpha + \frac{C_{D,W}}{2} \frac{S_W}{S_F} \left(\frac{V}{V_j} \right)^2 \quad (55)$$

A similar procedure is used to obtain the lift and drag coefficients of the combination. In this case, it is desirable to start by reducing the fan forces to the form of coefficients based on the wing; thus, from equation (51) and equations (26) and (23)

$$C_{L,F} = \frac{L_F \rho S_F V_j^2}{T_S \frac{\rho}{2} V^2 S_W} = \frac{2 \cos \alpha \frac{S_F}{S_W}}{\left(\frac{V}{V_j}\right)^2} \quad (56)$$

$$C_{D,F} = \frac{D_F \rho S_F V_j^2}{T_S \frac{\rho}{2} V^2 S_W} = \frac{2 \frac{S_F}{S_W}}{V/V_j} \left(1 + \frac{\sin \alpha}{V/V_j}\right) \quad (57)$$

The total lift and drag coefficients are then obtained by adding the wing lift and drag coefficients to equations (56) and (57)

$$C_{L,t} = C_{L,W} + \frac{2 \cos \alpha \frac{S_F}{S_W}}{\left(\frac{V}{V_j}\right)^2} \quad (58)$$

$$C_{D,t} = C_{D,W} + \frac{2 \frac{S_F}{S_W}}{V/V_j} \left(1 + \frac{\sin \alpha}{V/V_j}\right) \quad (59)$$

External drag-lift ratio. - The external drag-lift ratio is obtained by dividing equation (55) by equation (56) to yield

$$\left(\frac{D}{L}\right)_t = \frac{\frac{V}{V_j} + \sin \alpha + \frac{C_{D,W}}{2} \frac{S_W}{S_F} \left(\frac{V}{V_j}\right)^2}{\cos \alpha + \frac{C_{L,W}}{2} \frac{S_W}{S_F} \left(\frac{V}{V_j}\right)^2} \quad (60)$$

The identical expression, of course, would be obtained if equation (59) were divided by equation (58).

Equivalent lift-drag ratio.- Equation (40) gives the ratio of the equivalent drag to static thrust for the fan as

$$\frac{D_{se}}{T_S} = \frac{1 + \frac{V}{V_j} \sin \alpha}{V/V_j} \quad (61)$$

The equivalent lift-drag ratio can be written as

$$\left(\frac{L}{D_e}\right)_t = \frac{L_t/T_S}{\frac{D_{se}}{T_S} + \frac{D_t}{T_S}} \quad (62)$$

where L_t/T_S is obtained from equation (54), D_t/T_S from equation (55), and D_{se}/T_S from equation (61). Performing the indicated substitutions in equation (62) yields

$$\left(\frac{L}{D_e}\right)_t = \frac{\frac{V}{V_j} \left[\cos \alpha + \frac{C_{L,W}}{2} \frac{S_W}{S_F} \left(\frac{V}{V_j}\right)^2 \right]}{1 + 2 \frac{V}{V_j} \sin \alpha + \left(\frac{V}{V_j}\right)^2 + \frac{C_{D,W}}{2} \frac{S_W}{S_F} \left(\frac{V}{V_j}\right)^3} \quad (63)$$

As noted earlier, the expression given in equation (63) may not be appropriate to cases where there is a net propulsive thrust (or negative total drag). As noted earlier, the considerations which lead to equation (63) debit the total power by any power expended in producing a forward propulsive thrust. Depending upon the usage, when forward propulsive thrust is present, it may be preferable to take the shaft-equivalent drag as the total equivalent drag; that is, for $D_t/T_S < 0$,

$$\left(\frac{L}{D_e}\right)_t = \frac{L_t/T_S}{D_{se}/T_S} \quad (64)$$

or

$$\left(\frac{L}{D_e}\right)_t = \frac{\frac{V}{V_j} \left[\cos \alpha + \frac{C_{L,W}}{2} \frac{S_W}{S_F} \left(\frac{V}{V_j}\right)^2 \right]}{1 + \frac{V}{V_j} \sin \alpha} \quad (65)$$

To add equivalent drag to measured data.- In the case of wind-tunnel measurements, the total external drag, the lift, and the static thrust are known from the balance readings. Thus, in equations (62) and (64), the quantities L_t/T_S and D_t/T_S are already known from the tests. Thus,

$$\left(\frac{L}{D_e}\right)_t = \frac{L_M/T_S}{\frac{D_{se}}{T_S} + \frac{D_M}{T_S}} \quad (66)$$

or substituting equation (61) into equation (66)

$$\left(\frac{L}{D_e}\right)_t = \frac{\frac{V}{V_j} \frac{L_M}{T_S}}{1 + \frac{V}{V_j} \left(\sin \alpha + \frac{D_M}{T_S} \right)} \quad (67)$$

or, perhaps, in the case of propulsive thrust (negative D_M)

$$\left(\frac{L}{D_e}\right)_t = \frac{\frac{V}{V_j} \frac{L_M}{T_S}}{1 + \frac{V}{V_j} \sin \alpha} \quad (68)$$

It will be observed that the momentum theory does not include the profile drag of the fan blades; it does not consider any loss in efficiency caused by a nonuniform fan disk-load distribution (which is certainly the case for most configurations because of the large central fan boss); and it does not allow for any additional power transmission losses (caused by gearing or pressure losses in a pneumatic system). Thus, in practice, D_{se}/T_S must be expected to be considerably greater than its theoretical value, and the equivalent lift-drag ratio would be correspondingly less.

Effect of tail loads.- Properly speaking, the foregoing equations apply only to the fan-wing combination, and any effects caused by an altered lift and drag of the tail should be assessed separately and added to these results. Calculation of the tail loads requires a knowledge of the induced field of the combined lifting system at the location of the tail. Unfortunately, such a calculation is beyond the province of simple momentum theory. Consequently, the values used in the calculations in this paper have been based upon the

values of $C_{L,W}$ and $C_{D,W}$ which were measured for the complete model (including the fuselage and tail) with the fans covered and inoperative. This procedure is probably no worse than the neglect of the mutual interference between wing and fans and the neglect of the aforementioned losses in the fans themselves.

EXPERIMENT

Apparatus and Tests

Model.- The model used in this investigation is shown in figure 4 and pertinent dimensions are further detailed in tables I and II. The model consisted of a symmetrical streamline body 2.13-m long (84-in.) with a maximum diameter of 0.2-m (8-in.). A symmetrical tapered wing of 1.07-m (42-in.) span was mounted at the midpoint of the body. The airfoil section at the wing tip was NACA 16-015 and the section increased in thickness to a modified NACA 16-017 at the center line of the body; straight-line fairings were used between these two stations.

Two commercially available 0.2-m (8-in.) tip turbine driven fans were mounted on centers spaced 0.56 m (22 in.) apart at the mid-chord position of the wing. The inlets to these fans were of the simple bellmouth type obtained by providing a reasonable radius at the intersection of the fan duct and the upper wing surface.

A slab tail of 0.76-m (30-in.) span and 0.32-m (12.5-in.) chord was mounted symmetrically so that its trailing edge was coincident with the rearmost end of the fuselage.

The model was mounted on a pivot at the midpoint of the fuselage. (See fig. 5(a).) A linear actuator, installed between the mounting strut and a point further rearward on the model, provided remote control of angle of attack.

Instrumentation.- The model forces were measured by the standard mechanical balance of the wind tunnel. This balance was not designed for models as small as that of the present investigation and the measurement of moments by this balance was not feasible.

The rotational speed of the fans was measured by means of magnetic pickups provided within the fan casings. Angle of attack was measured by means of an accelerometer transducer mounted within the model.

Detailed examination of the data, together with the known capabilities of the external balance, indicates that the lift measurements should be accurate to within ± 13 N (± 3 lb), and the drag measurements should be accurate to within ± 4.4 N (± 1 lb). Dynamic pressure is believed to be accurate to within 1 percent, and angle of attack is believed to be accurate to within 0.1° .

Wind tunnel and model installation.- The wind tunnel used was the Langley full-scale tunnel which has a nominal test section size of 9.14 by 18.3 m (30 by 60 ft). This tunnel

is described in reference 25. Some later information on the wind tunnel is presented in references 26 and 27.

The groundboard normally used in the Langley full-scale tunnel was in place during these tests. The upper surface of this groundboard is approximately 0.61 m (2 ft) above the lower edge of the jet boundary; thus, the cross-sectional area of the test section is reduced to 141.8 m² (1527 ft²). By comparison, the model is very small; its wing area being less than one-half of 1 percent of the test-section cross-sectional area.

The model was mounted on a special strut so that it was centered vertically in the active region of the test section (4.26 m (14 ft) above the groundboard). A close-fitting streamlined fairing was installed around the strut starting 1.07 m (3.5 ft) below the model and continuing downward to meet the groundboard. All air lines and electrical loads were dressed as closely to the strut as possible. Photographs of the model mounted in the wind tunnel are presented in figure 5.

The air-pressure lines were brought across the mechanical balance in a trapeze arrangement. Tests conducted under pressure with the hoses blocked at the model indicated no effect on the balance readings. The instrument leads were carried across the balance by means of a large hanging loop.

Prior to mounting the model on the strut, the region occupied by the model was surveyed with a pitot-static-pitch-yaw head. The dynamic pressure measured by this survey instrument was used to calibrate the velocity at the model location as a function of static depression in the tunnel setting chamber; this static depression, in turn, was used to determine the tunnel velocity during the tests. The survey also disclosed the presence of a significant stream angle at the model location. The presence of this stream angle was confirmed later by the raw data from the symmetrical model when it was tested with the fans covered. The effects of this stream angle have been removed from all the data presented herein.

The Langley full-scale tunnel does not have continuous speed control throughout the velocity range covered in these tests; instead, it has some 24 discrete power settings or "points." A number of these points appropriate to the desired speed range were selected. The actual velocity presented herein was determined from the average of no fewer than 10 samplings, spaced 1-second apart, of the static depression.

Comparison Between Experiment and Theory

Lift.- The ratio of lift to static thrust as calculated from equation (54) is compared with the wind-tunnel measurements in figure 6. As a matter of orientation as to the quantitative significance of the values of V/V_j given in the abscissa of this figure, it might be observed that values between 0 and approximately 0.5 represent the range of

transition speeds for practical VTOL aircraft. Greater values of V/V_j correspond to speeds at which a VTOL aircraft would be expected to be wingborne and consequently are of little significance. The data of figure 6 show that at values of V/V_j above 0.5, there is evidently significant favorable interference between the wing and the fans; however, within the usable range of transition speeds the theoretical prediction of L/T_S is in reasonable agreement with the measurements. In this latter range there is a small lift loss (5 to 10 percent) presumably caused by mutual interference.

Drag. - Because of the relatively large drag of the exposed strut, all drags presented herein are measured from the drag at $\alpha = 0^\circ$. Thus, these drags are approximately those due to lift. The ratio of drag to static thrust (from eq. (55)) and the external drag-lift ratio (from eq. (60)) are compared with the wind-tunnel measurements in figures 7 and 8.

Momentum theory is based on an idealized situation in which the drag should be somewhat less than the actual observed drag. In general, this result is obtained throughout figures 7 and 8. At high speeds, D/L is better (that is, less) than that predicted because of the favorable mutual interference discussed in the preceding section. (See fig. 8.)

Equivalent lift-drag ratio. - No measurements adequate to define the actual "shaft" power were made during the wind-tunnel tests. In any event such measurements would have been meaningless in terms of a full-scale aircraft because of the poor efficiency of the model fans. Instead, the calculated drag equivalent of the shaft power (eq. (40)) has been added to the measured external drag to provide an equivalent lift-drag ratio (eq. (67)) and compared with the theoretical values (eq. (63)) in figure 9.

The most notable feature of figure 9 is the very low efficiency of the fan-in-wing system. This low efficiency is fully confirmed by sample calculations made using the measured shaft powers presented in reference 11. Even helicopter rotors at similar forward velocities tend to produce equivalent lift-drag ratios an order of magnitude greater than those shown in figure 9. It is obvious that the large disk loading of fan lift configurations will require large installed power in hover; however, the meager values of L/D_e indicate in a single term that the large installed power and heavy fuel-flow requirements will continue throughout transition.

Transition from hover to forward flight with full conversion may only require a few minutes and, therefore, may not consume a major portion of the available fuel. The real problem may occur in the landing transition. If it is necessary, because of weather or other reasons, to perform an instrument approach to a landing in relatively confined quarters, the time spent in a transitional mode of flight may become significantly great. Under such conditions, the fuel consumption in landing will be large. Even the fuel

reserves required for the possible need of an instrument landing could constitute a major range penalty for commercial configurations.

Equation (44) indicates that the isolated lifting fans should have greater values of L/D_e at negative angles of attack than at positive angles of attack. For the complete configuration, figure 9 shows that the opposite trend exists. The reason for this trend is simply the lift of the wing which is negative for $\alpha < 0$ and positive for $\alpha > 0$. Even a wing of aspect ratio 1.6, such as that of the present model, is a far more efficient lifting device than the fan.

"FAN-INDUCED" LIFT

Although the appendix indicates the possibility of favorable interference, it is significant that figure 6 does not indicate the large favorable "fan-induced" lifts which have been taken in the past as indicating substantial advantages for fan lift configurations. (See refs. 3 and 10.) Indeed, the possibility that such fan-induced lift is overstated has already been raised by references 13 and 14 where small models in the Langley full-scale tunnel did not obtain the same favorable result as prior large-scale tests. (See particularly figs. 26 to 29 of ref. 14.)

Reference 15 presents the results of a comprehensive experimental study of the effect of wall interference on the present model. In addition to the test reported on herein, the model was also tested in a series of smaller test sections. The measured ratios of L/T_S obtained in the investigation of reference 15 are shown in figure 10.

It is evident in figure 10 that as the cross-sectional area of the test section was decreased, the measured value of L/T_S increased. Whereas the results obtained in the Langley full-scale tunnel uniformly indicate small losses due to interference throughout the usable transition-speed range $V/V_j < 0.5$, the measured data in the smaller test sections uniformly indicate large increases in lift. The data obtained in the 1.12- by 2.24-m (44- by 88-in.) flat-oval test section are particularly significant since the model in that section has essentially the same ratio of model span to tunnel width (which is shown in ref. 15 to be the pertinent scaling parameter) as did the models of references 3 to 10. Indeed, reference 15 has shown that the wall-induced gain in lift in the small section correlates very well with the fan-induced lift of those investigations. It is further evident that for this model even simple momentum concepts provide a more reasonable estimate of the actual performance than that obtained from wind-tunnel tests in which the model span approaches half the width of the tunnel.

In view of the results of reference 15, it must be assumed that the fan-induced lift of references 3 to 10 resulted primarily from wall-interference which was not properly accounted for in reducing the data. Proper application of corrections for wall interference

can avoid difficulties of this nature. Figure 11 presents the same data corrected for wall interference by the method of references 28 and 29. If the magnitude of the corrections (in which correction angles as great as 14° were required) is considered, the theoretical corrections appear to correlate in a satisfactory manner the data from all the test sections.

The data for the present model, together with the discussion in the appendix, indicate that the fans were located in a fairly neutral position insofar as fan-induced lift is concerned. The discussion in the appendix indicates that favorable interaction between the fans and wing could be anticipated if the fans had been located at the trailing edge of the wing. Such a rearward location would present considerable difficulty in providing a proper moment balance of the aircraft in VTOL flight. The solution to the moment problem requires either a tail fan (with a consequent downward thrust) or other fans located forward of the wing. The appendix indicates that locating fans forward of the wing could result in serious fan-induced losses.

The amount of favorable interference that can be generated by judicious location of the main lifting and the balancing fans cannot now be predicted. A few jet VTOL configurations have exhibited slightly favorable characteristics; however, there is ample evidence to indicate that the opposite trend – large adverse interference effects – can be encountered.

CONCLUDING REMARKS

A simple incompressible-flow momentum theory presented herein includes many of the known experimentally determined characteristics of lifting-fan aircraft. These characteristics include the negligible effect of forward speed on fan thrust, the large momentum drag, and the generally inefficient performance throughout the transition-speed range. Although mutual interference between the fans and the wing was totally neglected, the theory is confirmed by experimental results for the configuration of the present tests. Examination of the results of an investigation of wall interference leads to the conclusion that the large fan-induced lift reported in many earlier investigations was largely the result of neglecting wall interference in the reduction of wind-tunnel data.

Langley Research Center,
National Aeronautics and Space Administration,
Hampton, Va., November 19, 1973.

APPENDIX

QUALITATIVE ASSESSMENT OF MUTUAL INTERFERENCE BETWEEN WING AND FANS

It is often possible to obtain some insight into interference effects by considering known results from other studies on only grossly similar systems. Such a qualitative assessment is particularly important in the case of the fan-in-wing configuration, since, as noted in the main text, there are conflicting claims as to the nature and magnitude of this interference.

This appendix uses, as a basis of discussion, the calculated induced flow field of a helicopter rotor. (See refs. 30-33.) In the case of a rotor, these calculations have been reasonably well verified by the measurements of reference 31 in forward flight, even though there are some problems apparent near hovering where the induced velocities are the only velocities present. (See ref. 34.) The rotor flow field is modified by the existence of a wing surrounding the rotor; however, the more obvious modifications are the very factors which lead to the mutual interference.

Symbols

R	rotor radius
u	induced velocity component directed along the X-axis (along longitudinal axis of rotor tip-path plane), positive rearward
V	forward-flight velocity
V_j	fan-efflux velocity
w	induced velocity directed along Z-axis (normal to tip-path plane), positive upward
w_0	mean, or momentum theory, value of w, positive upward
X,Y,Z	Cartesian coordinate system centered in rotor tip-path plane, X positive rearward, Z positive upward, Y laterally to form a right-hand coordinate system; also distances along these axes
α	tip-path plane angle of attack, angle between relative wind and X-axis, positive with leading edge up, deg

APPENDIX – Continued

λ	rotor tip-path plane inflow ratio,	$\frac{V \sin \alpha + w_0}{\Omega R}$
μ	rotor tip-speed ratio,	$\frac{V \cos \alpha}{\Omega R}$
χ	wake skew angle, angle between negative Z-axis and center of wake, positive rearward (note that, in contrast to remainder of this paper, χ is defined from axis of tip-path plane rather than from lift-drag axes), $\tan \chi = -\mu/\lambda$, deg	
Ω	rotor rotational speed, rad/sec	

Rotor-Induced Velocities

Charts presenting the normal (w) component of induced velocity will be found in numerous papers and a summary of these charts is found in reference 32. The longitudinal (u) component of induced velocity has received lesser attention; however, it is important in the present case. This component may be obtained by numerical integration of the equations of reference 33 (noting an error in sign for the u -component in that paper). Indeed, subroutines suitable for the calculation are included as subroutines RTRLQAD and ROTVEL in appendix C of reference 35.

Because of the paucity of published information, these calculations have been made for a rotor with uniform disk loading. The results are presented in figure 12 for increments of 10° in wake skew angle. Reference 31 demonstrates that the disk-load distribution has a significant effect on the flow field and a few results for a triangular disk-load distribution are presented in figure 13.

Although a comparison of figures 12 and 13 indicates large differences in the field in the central plane of the rotor, it should not be necessary to consider this effect in the present analysis for two reasons. First, the analysis is purely qualitative. Second, reference 36 has shown that the calculated field in the central plane of a uniformly loaded rotor is a reasonably good representation of the average field across the span of the rotor.

The induced-velocity fields given in figures 12 and 13 are independent of angle of attack and depend only upon the wake skew angle. However, the induced velocities are not the only velocities present in forward flight. The actual flow will be the vectorial sum of the induced velocities and the forward-flight velocity. This vectorial sum may differ dramatically as a function of angle of attack. The effect is shown for one wake skew angle in figure 14. Additional examples are available throughout reference 35.

APPENDIX – Continued

Fan In Wing

The presence of a wing surrounding the rotor or fan will drastically alter the flow fields given in figures 12 and 13 since no flow can pass through the wing surface. In the present case, the wing extends more than 2 radii ahead of and behind the central plane of the fan. Furthermore, at high speed the wake of the fan will take on a drastically curved character (ref. 37) rather than the linear shape assumed as the basis for the calculated field. Finally, as observed in the main text, the fan efflux at the exit will always be directed along the fan axis.

The last named two differences may be accounted for by assuming that the curved wake, emanating normal to the wing, may be represented by a linear wake having some effective skew angle. In hovering, this effective skew angle would be 0° . In forward flight, however, the wake is rapidly turned rearward, and by the time V/V_j has reached a value of a few tenths, the effective skew angle should be on the order of 40° to 70° . Since the apparent favorable interference for the fan-in-wing configuration increases with speed, this is the range of wake skew angles which will be of interest.

The effect of the wing in altering the flow field is of greater interest, since it is by means of these alterations that the mutual fan-wing interference is generated. First, consider the effect of the normal component of induced velocity. Over the forward part of the wing, which lies at $Z = 0$ and $X/R < 1$, there is an upwash ($w/w_0 < 0$) which becomes somewhat greater as the wake skew angle increases. (See fig. 12.) Over the rearward part of the wing ($Z = 0$, and $X/R > 1$), figure 12 indicates a powerful downwash which becomes more intense as the wake skew angle increases.

The aforementioned upwashes and downwashes are destroyed by the presence of the wing surface. However, in stopping these flows, pressures are generated at the surface of the wing. The action is much the same as the means by which the wake of an aircraft transfers the weight of the aircraft to the surface of the Earth. (See ref. 38.) Thus, the fan field will produce an upload on the forward part of the wing and a download on the rearward part of the wing. Consequently, it would be expected that the longitudinal placement of the fan in the wing should have a powerful effect on the interference. Even in the face of enormous wall interference, this effect stands out clearly in the data correlation of reference 3.

The downwash field on the rearward part of the wing may become very strong. Indeed, this field is sufficiently strong that one would anticipate that the flow would separate below this part of the wing. Such separation has been observed in the wind tunnel. (See fig. 7 of ref. 3.) In view of the large downwash field indicated by figure 12, this separation may actually help by limiting the degree of download carried on the rear of the wing.

APPENDIX – Continued

Although not shown in figures 12 to 14, there is an upwash beyond the lateral tips of a rotor. (See refs. 30 to 32.) This upwash field increases with the wake skew angle. Again, this laterally disposed upwash should provide some upload on the surfaces of the wing alongside the fan.

The longitudinal induced velocities of figure 12 are also of interest. Observe that since w_0 is negative for positive lift, negative values of u/w_0 represent rearward velocities, and positive values of u/w_0 represent forward velocities. Over the forward part of the wing there is a rearward-directed velocity which adds to the velocities already present on the wing surfaces, and which further increases the lift. The vertical gradient of the field in this region is such that for a wing section of substantial thickness with respect to the fan radius, an increase in circulation would be created. Furthermore, the wing in stopping the vertical induced velocities turns the flow, and the direction of the turn is largely determined by the velocities already present on the surface. This effect should further increase the velocities along the surface with a consequent further increase in lift. The sum of all these various effects can result in very high local velocities and a very substantial increase in the lift of the forward part of the wing. The large local pressures are clearly seen in the pressure-distribution measurements of reference 5. (It should be observed, however, that the data of ref. 5 are not corrected for wall effects; thus, part of the effects shown therein is caused by a significant wall-induced increase in the wing angle of attack caused by operation of the fans within the test section.)

Behind the fans, figure 12 indicates forward-directed induced velocities of large magnitude. If V_j is taken as being approximately w_0 and V/V_j is assumed to range between, say, 0.3 to 0.5, the values shown in figure 12 lead to the conclusion that the flow should be reversed over large parts of the wing behind the fans. The flow sketch of figure 7 in reference 3 clearly indicates this probability.

Flow reversal, with the probable consequence of flow separation from the upper surface, should substantially mitigate the downloads on the rear of the wing. Nevertheless, it is clear that at least at the lower speeds, a download must exist in this region. For example, reference 12 clearly shows that at low speed the center of pressure of the fan-wing combination moves to a location forward of the leading edge of the wing. A shift of this magnitude is possible only if there is a download on the rear of the wing.

The actual interference obtained will be a balance between the conflicting effects described. At low speed, the existence of centers of pressure far forward of the fan center, and even ahead of the wing, suggests that the losses on the rear of the wing are larger than the gains to be obtained on the forward part of the wing. Thus, at low speed, the mutual interference should be harmful. Certainly, this is the result of the present investigation (fig. 6) throughout the transition range ($V/V_j < 0.5$). At higher speeds, where the dynamic pressure is much greater, it is possible for the gain on the forward part of

APPENDIX -- Concluded

the wing to be greater than the losses behind the fan. This effect was also found in the present investigation; however, it only occurred at speeds too great for transition.

The moments arising from the mutual interference are a powerful influence on the possible practical arrangements of fan-in-wing configurations. The aircraft, when fully converted, must fly as a conventional aircraft with its center of gravity somewhere in the vicinity of the quarter chord of the wing. In hovering, it must also be capable of being trimmed about this same center of gravity. If designed only to hover, the obvious choice of a fan location would be near the quarter chord. Unfortunately, the large nose-up moments in transition, together with considerations of mutual interference effects, necessitate a more rearward fan location. Thus, a powerful means of pitch control such as an additional fan is required to balance the aircraft in hover. Because a tail location for this fan would involve a significant download and reduce the lift, the pitch-control fan is placed in the nose. The forward location of this fan results in lift losses in transition caused by the mutual interference between the fan and the fuselage surfaces, and efficiency is lost once more.

An alternate approach is to increase the number of fans so that two can be placed forward of the wing and two behind, or near, the trailing edge of the wing. The relative efficiency of the fans will be rather different depending upon their location; however, the combination is likely to have no better efficiency than the simpler arrangement.

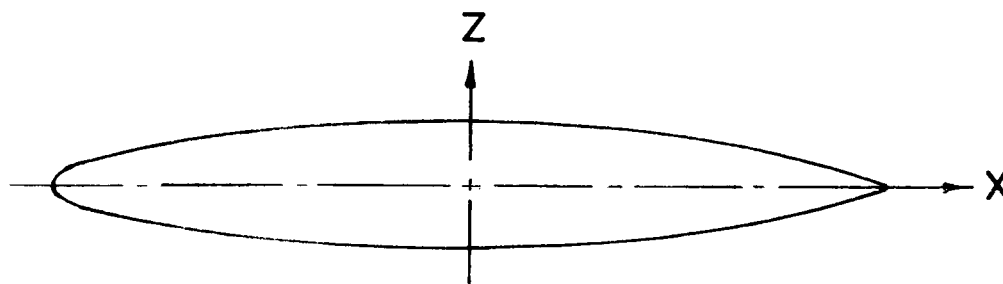
REFERENCES

1. Deckert, Wallace H.; and Evans, Robert C.: NASA Lift Fan Transport Technology Status. [Preprint] 720856, Soc. Automot. Eng., Oct. 1972.
2. Eldridge, W. M.; Ferrell, J. A.; McKee, J. W.; Wayne, J. F., Jr.; and Zabinsky, J. M.: Conceptual Design Studies of Candidate V/STOL Lift Fan Commercial Short Haul Transport for 1980-85 V/STOL Lift-Fan Study. NASA CR-2183, 1973.
3. Hickey, David H.; and Cook, Woodrow L.: Aerodynamics of V/STOL Aircraft Powered by Lift Fans. Fluid Dynamics of Rotor and Fan Supported Aircraft at Subsonic Speeds, AGARD CP No. 22, Sept. 1967, pp. 15-1 - 15-17.
4. Aoyagi, Kiyoshi; Hickey, David H.; and deSavigny, Richard A.: Aerodynamic Characteristics of a Large-Scale Model With a High Disk-Loading Lifting Fan Mounted in the Fuselage. NASA TN D-775, 1961.
5. Hickey, David H.; and Hall, Leo P.: Aerodynamic Characteristics of a Large-Scale Model With Two High Disk-Loading Fans Mounted in the Wing. NASA TN D-1650, 1963.
6. Kirk, Jerry V.; Hickey, David H.; and Hall, Leo P.: Aerodynamic Characteristics of a Full-Scale Fan-In-Wing Model Including Results in Ground Effect With Nose-Fan Pitch Control. NASA TN D-2368, 1964.
7. Hall, Leo P.; Hickey, David H.; and Kirk, Jerry V.: Aerodynamic Characteristics of a Large-Scale V/STOL Transport Model With Lift and Lift-Cruise Fans. NASA TN D-4092, 1967.
8. Kirk, Jerry V.; Hodder, Brent K.; and Hall, Leo P.: Large-Scale Wind-Tunnel Investigation of a V/STOL Transport Model With Wing-Mounted Lift Fans and Fuselage-Mounted Lift-Cruise Engines for Propulsion. NASA TN D-4233, 1967.
9. Dickinson, Stanley O.; Hall, Leo P.; and Hodder, Brent K.: Aerodynamic Characteristics of a Large-Scale V/STOL Transport Model With Tandem Lift Fans Mounted at Mid-Semispan of the Wing. NASA TN D-6234, 1971.
10. Kirk, Jerry V.; Hall, Leo P.; and Hodder, Brent K.: Aerodynamics of Lift Fan V/STOL Aircraft. AIAA Paper No. 71-981, Oct. 1971.
11. Schaub, Uwe W.; and Bassett, Robert W.: Flow Distortion and Performance Measurements on a 12" Fan-in-Wing Model for a Range of Forward Speeds and Angle of Attack Settings. Inlets and Nozzles for Aerospace Engines, AGARD CP No. 91-71, 1971, pp. 17-1 - 17-13.

12. Wardlaw, R. L.; and Templin, R. J.: Preliminary Wind Tunnel Tests of a Lifting Fan in a Two-Dimensional Aerofoil. Lab. Rep. LR-207, Nat. Aeronaut. Estab. Canada, Sept. 1957.
13. Newsom, William A., Jr.; and Moore, Frederick L.: Wind-Tunnel Investigation of a V/STOL Transport Model With Six Wing-Mounted Lift Fans. NASA TN D-5695, 1970.
14. Newsom, William A., Jr.: Wind-Tunnel Investigation of a V/STOL Transport Model With Four Pod-Mounted Lift Fans. NASA TN D-5942, 1970.
15. Heyson, Harry H.: The Effect of Wind-Tunnel Wall Interference on the Performance of a Fan-in-Wing VTOL Model. NASA TN D-7518, 1974.
16. Heyson, Harry H.: Nomographic Solution of the Momentum Equation for VTOL-STOL Aircraft. NASA TN D-814, 1961. (Also available as: V/STOL Momentum Equation, Space/Aeron. vol. 38, no. 2, July 1962, pp. B-18 to B-20.)
17. Heyson, Harry H.: A Note on the Mean Value of Induced Velocity for a Helicopter Rotor. NASA TN D-240, 1960.
18. Newsom, William A., Jr.: Wind-Tunnel Investigation of a Deflected-Slipstream Cruise-Fan V/STOL Aircraft Wing. NASA TN D-4262, 1967.
19. Templin, R. J.: A Momentum Rule for Optimum Aircraft Performance in the V/STOL Transition Regime. Aeronaut. Rep. LR-470, Nat. Aeronaut. Estab. Canada, Jan. 1967.
20. Glauert, H.: A General Theory of the Autogyro. R. and M. No. 1111, British A. R. C., 1926.
21. Prandtl, L.: Applications of Modern Hydrodynamics to Aeronautics. NACA Rep. 116, 1921.
22. Wald, Quentin: A Method for Rapid Estimation of Helicopter Performance. Jour. Aeron. Sci., vol. 10, no. 4, Apr. 1943, pp. 131-135.
23. Coleman, Robert P.; Feingold, Arnold M.; and Stempin, Carl W.: Evaluation of the Induced-Velocity Field of an Idealized Helicopter Rotor. NACA WR L-126, 1945. (Formerly NACA ARR L5E10.)
24. Heyson, Harry H.: Wind-Tunnel Wall Effects at Extreme Force Coefficients. Ann. N.Y. Acad. Sci., vol. 154, art. 2, Nov. 22, 1968, pp. 1074-1093.
25. DeFrance, Smith J.: The NACA Full-Scale Wind Tunnel. NACA Rep. 459, 1933.
26. Schaefer, William T., Jr.: Characteristics of Major Active Wind Tunnels at the Langley Research Center. NASA TM X-1130, 1965.

27. Pirrello, C. J.; Hardin, R. D.; Heckart, M. V.; and Brown, K. R.: An Inventory of Aeronautical Ground Research Facilities. Vol. I - Wind Tunnels. NASA CR-1874, 1971.
28. Heyson, Harry H.: Linearized Theory of Wind-Tunnel Jet-Boundary Corrections and Ground Effect for VTOL/STOL Aircraft. NASA TR R-124, 1962.
29. Heyson, Harry H.: Use of Superposition in Digital Computers To Obtain Wind-Tunnel Interference Factors for Arbitrary Configurations, With Particular Reference to V/STOL Models. NASA TR R-302, 1969.
30. Castles, Walter, Jr.; and De Leeuw, Jacob Henri: The Normal Component of the Induced Velocity in the Vicinity of a Lifting Rotor and Some Examples of Its Application. NACA Rep. 1184, 1954. (Supersedes NACA TN 2912.)
31. Heyson, Harry H.; and Katzoff, S.: Induced Velocities Near a Lifting Rotor With Non-uniform Disk Loading. NACA Rep. 1319, 1957. (Supersedes NACA TN 3690 by Heyson and Katzoff and TN 3691 by Heyson.)
32. Jewel, Joseph W., Jr.; and Heyson, Harry H.: Charts of the Induced Velocities Near a Lifting Rotor. NASA MEMO 4-15-59L, 1959.
33. Heyson, Harry H.: Equations for the Induced Velocities Near a Lifting Rotor With Nonuniform Azimuthwise Vorticity Distribution. NASA TN D-394, 1960.
34. Heyson, Harry H.: Evaluation of Linearized Vortex Theory as Applied to Single and Multiple Rotors Hovering In and Out of Ground Effect. NASA TN D-43, 1959.
35. Heyson, Harry H.: Theoretical Study of Conditions Limiting V/STOL Testing in Wind Tunnels With Solid Floor. NASA TN D-5819, 1970.
36. Heyson, Harry H.: Preliminary Results From Flow-Field Measurements Around Single and Tandem Rotors in the Langley Full-Scale Tunnel. NACA TN 3242, 1954.
37. Margason, Richard J.: The Path of a Jet Directed at Large Angles to a Subsonic Free Stream. M.S. Thesis, Virginia Polytechnic Inst., May 1968. (Also available as NASA TN D-4919, 1968.)
38. Prandtl, L.; and Teitjens, O. G. (J. P. Den Hartog, trans.): Applied Hydro- and Aeromechanics. Dover Pub., Inc., 1957.

TABLE I
AIRFOIL ORDINATES

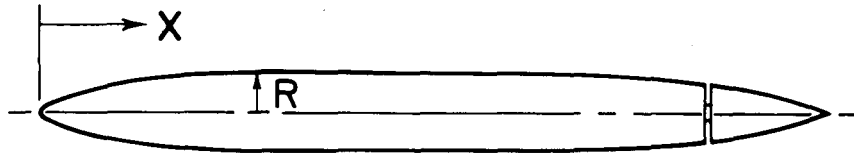


NACA 16-015

MODIFIED NACA 16-017

Sta. A; c=45.72 cm		Sta. A; c=18.00"		C _L sta.; c=83.414 cm		C _L sta.; c=32.84"	
X, cm	±Z, cm	X, in.	±Z, in.	X, cm	±Z, cm	X, in.	±Z, in.
-22.860	0	-9.000	0	-41.707	0	-16.42	0
-22.288	.739	-8.775	.291	-40.640	1.521	-16.00	.599
-21.717	1.031	-8.550	.406	-39.624	2.126	-15.60	.837
-20.574	1.435	-8.100	.565	-37.567	2.957	-14.79	1.164
-19.431	1.732	-7.650	.682	-35.458	3.571	-13.96	1.406
-18.288	1.976	-7.200	.778	-33.350	4.074	-13.13	1.604
-16.002	2.362	-6.300	.930	-29.210	4.862	-11.50	1.914
-13.716	2.664	-5.400	1.049	-25.019	5.497	- 9.85	2.164
- 9.144	3.096	-3.600	1.219	-16.688	6.386	- 6.57	2.514
- 4.572	3.345	-1.800	1.317	- 8.331	6.896	- 3.28	2.715
0	3.429	0	1.350	0	7.069	0	2.783
4.572	3.335	1.800	1.313	8.331	6.876	3.28	2.707
9.144	3.012	3.600	1.186	16.688	6.208	6.57	2.444
13.716	2.400	5.400	.945	25.019	4.945	9.85	1.947
18.288	1.438	7.200	.566	33.350	2.967	13.13	1.168
20.574	.808	8.100	.318	37.567	1.651	14.79	.650
22.860	.069	9.000	.027	41.707	.142	16.42	.056
Leading-edge radius: 0.503 cm (0.198")				Leading-edge radius: 0.917 cm (0.361")			

TABLE II
FUSELAGE ORDINATES



X, cm	Radius, cm	X, in.	Radius, in.
0	0	0	0
1.70	2.18	0.67	0.86
3.38	3.05	1.33	1.20
6.78	4.24	2.67	1.67
10.16	5.13	4.00	2.02
13.54	5.87	5.33	2.31
20.32	7.01	8.00	2.76
27.10	7.90	10.67	3.11
40.64	9.17	16.00	3.61
54.18	9.40	21.33	3.70
67.74	10.16	26.67	4.00
↓	↓	↓	↓
145.62	10.16	57.33	4.00
159.18	9.88	62.67	3.89
172.72	8.92	68.00	3.51
186.26	7.11	73.33	2.80
199.82	4.27	78.67	1.68
206.58	2.39	81.33	0.94
213.36	.20	84.00	0.08

Nose radius: 1.50 cm (0.59 in.)

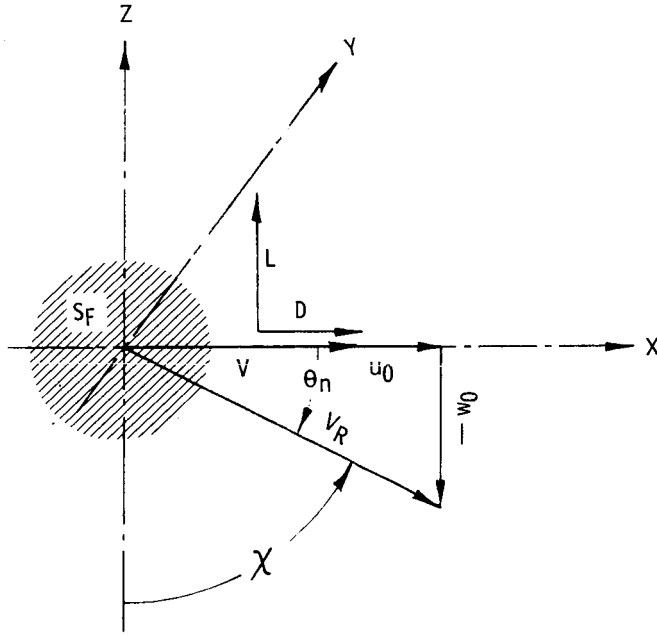


Figure 1.- Force and velocity vectors at aircraft.

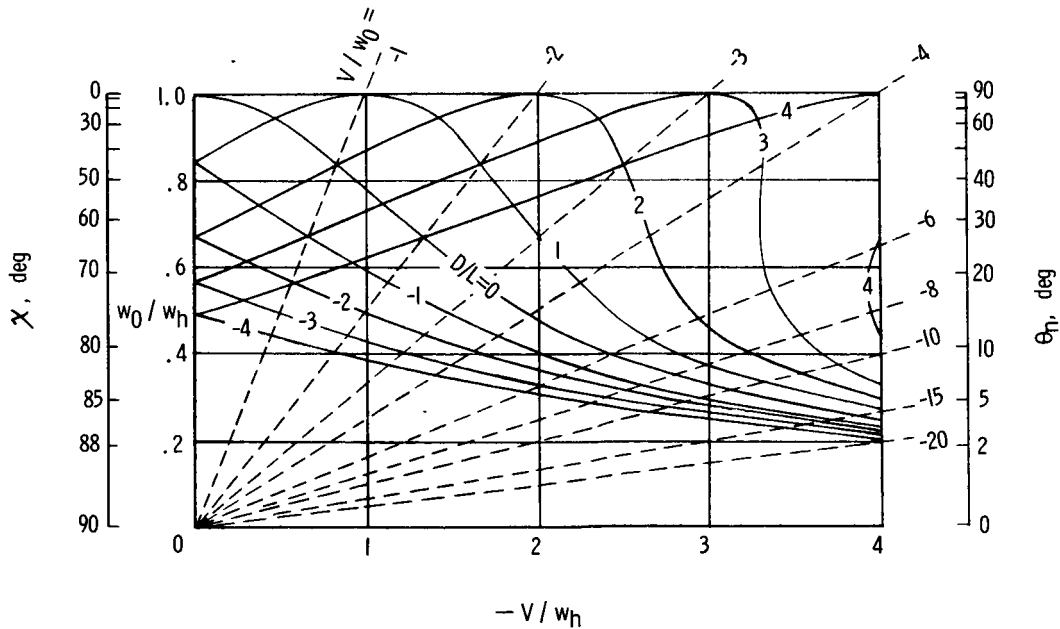


Figure 2.- Generalized momentum-theory chart according to reference 16. Chart shows w_0/w_h as a function of V/w_h for various values of D/L . Auxiliary scales showing the wake skew angle and the net downwash angle θ_n are included.

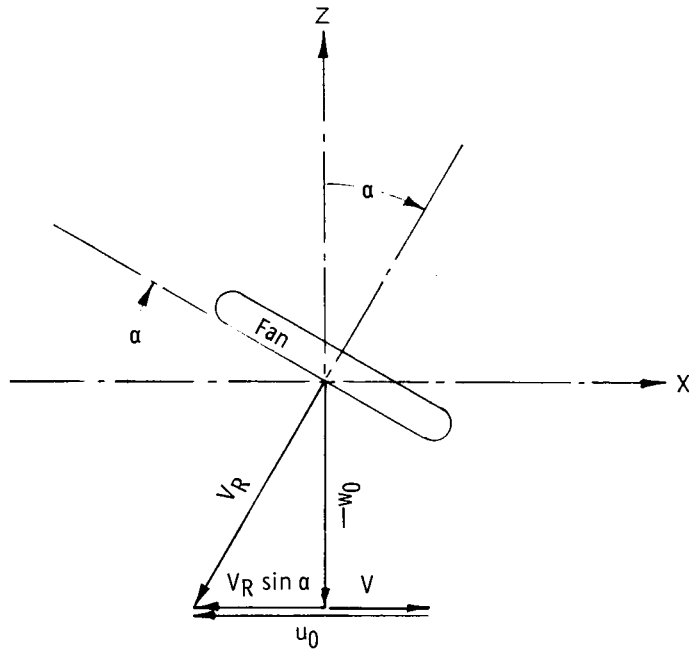


Figure 3.- Flow vectors at lifting fan.

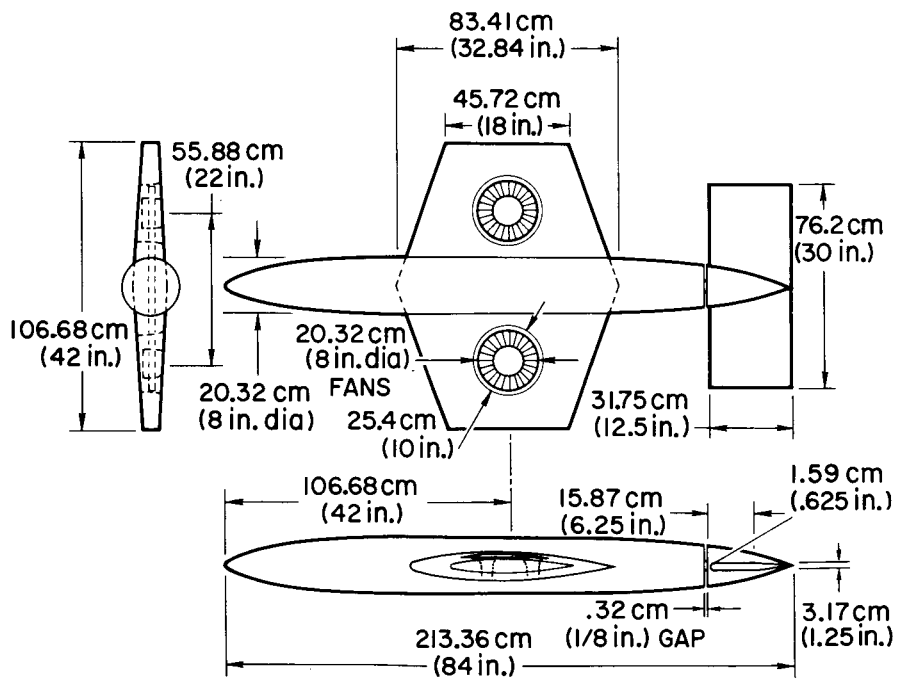
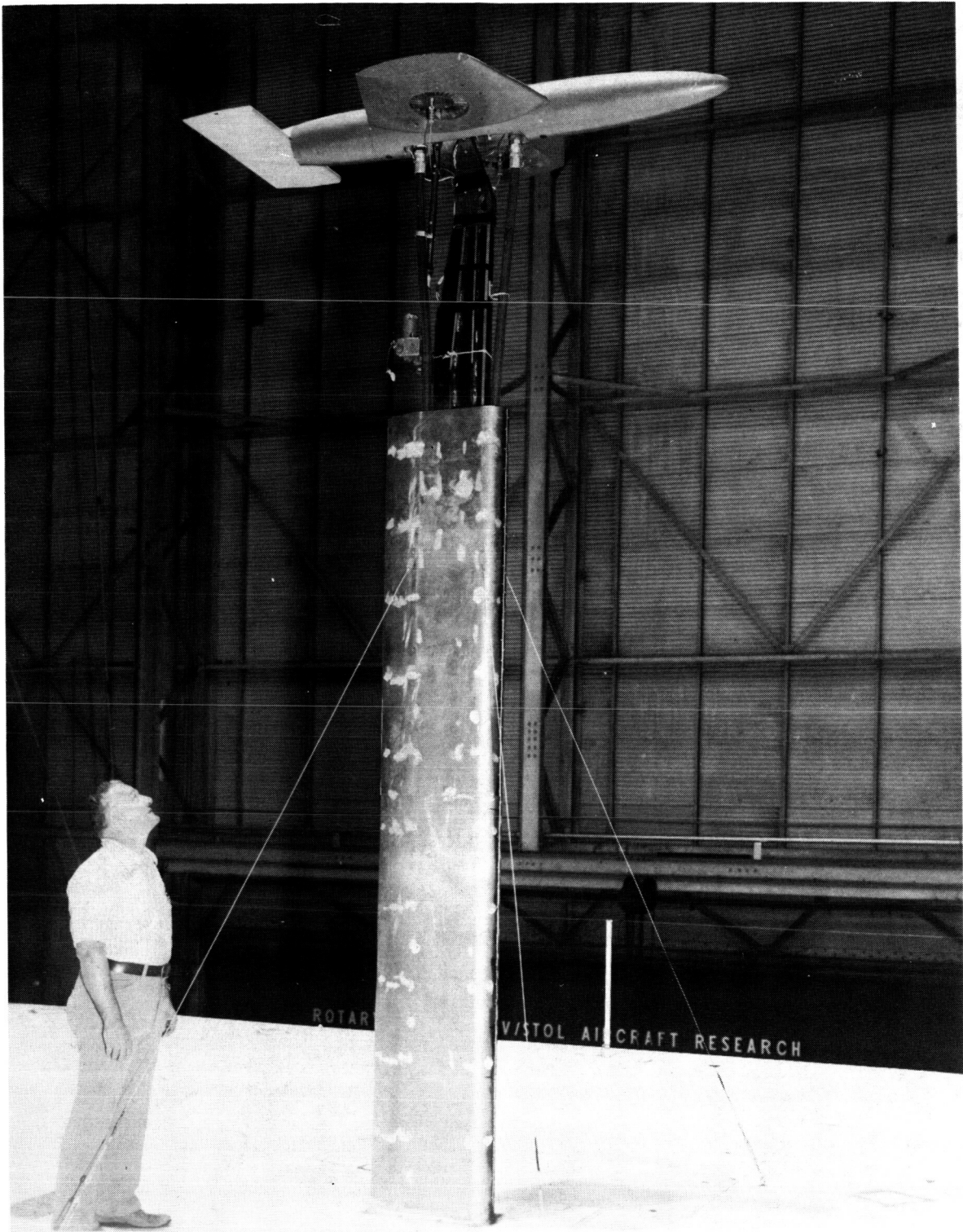


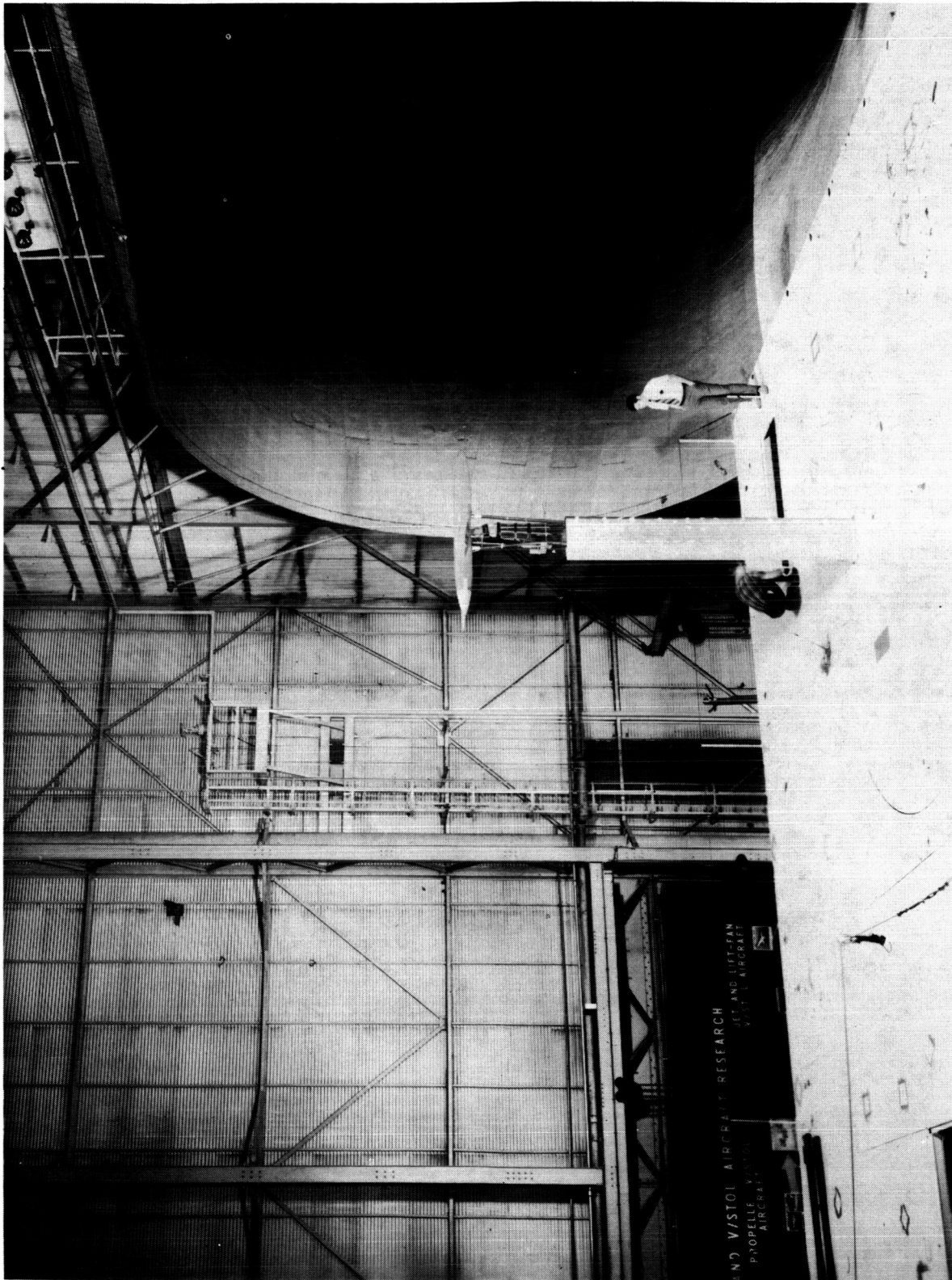
Figure 4.- Dimensional characteristics of model.



L-72-2844

(a) Near view.

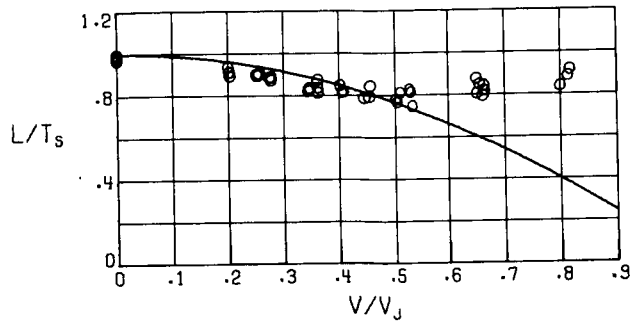
Figure 5.- Fan-in-wing model mounted in Langley full-scale wind tunnel.



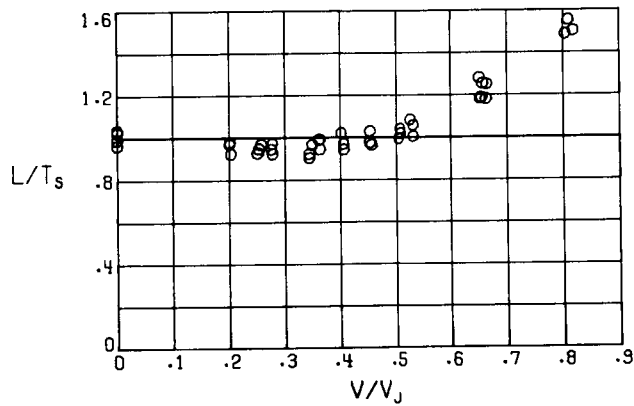
L-72-2843

(b) Distant view.

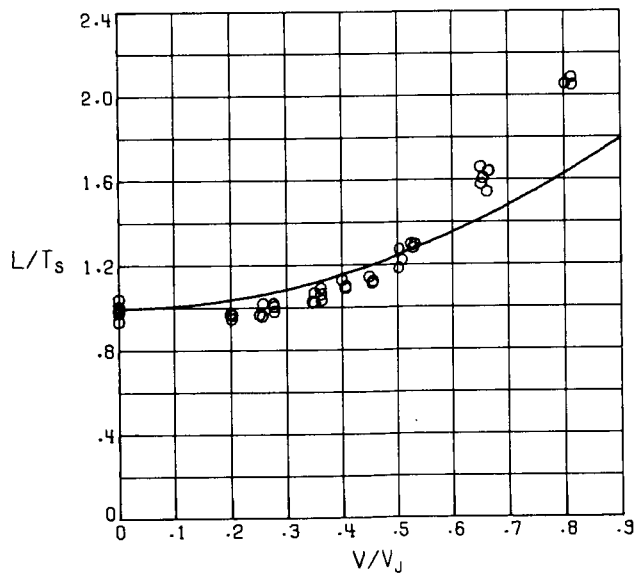
Figure 5. - Concluded.



(a) $\alpha = -5^\circ$.

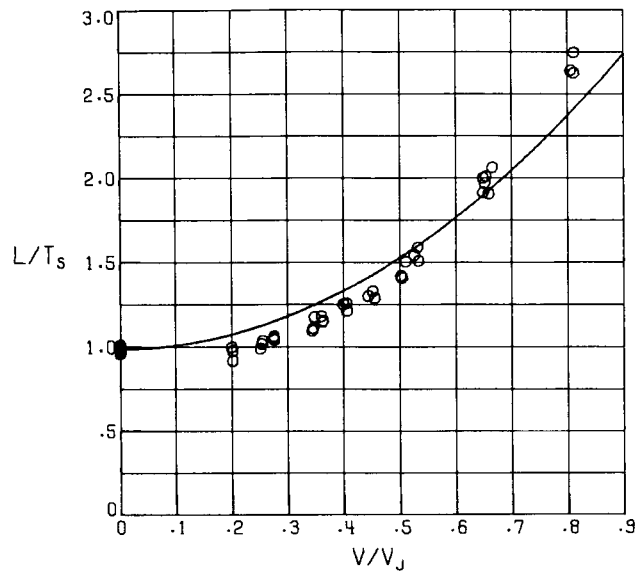


(b) $\alpha = 0^\circ$.

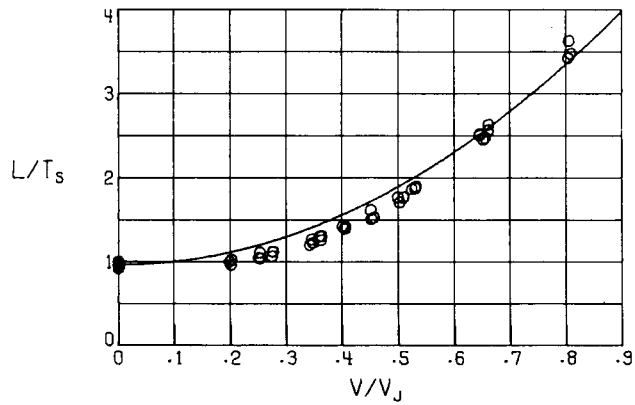


(c) $\alpha = 5^\circ$.

Figure 6.- Measurements of ratio of lift to static thrust for a small fan-in-wing model tested in Langley full-scale wind tunnel. The theoretical curve is calculated from equation (54).

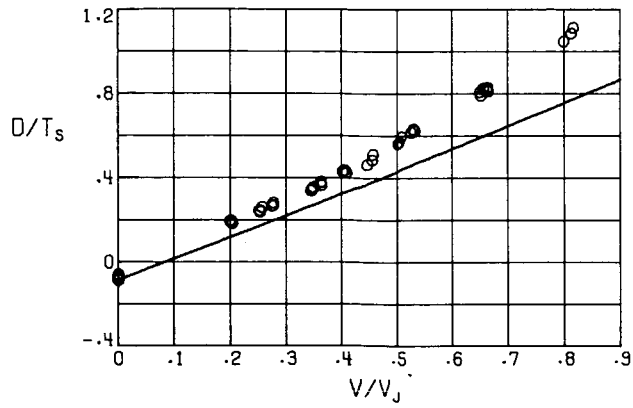


(d) $\alpha = 10^\circ$.

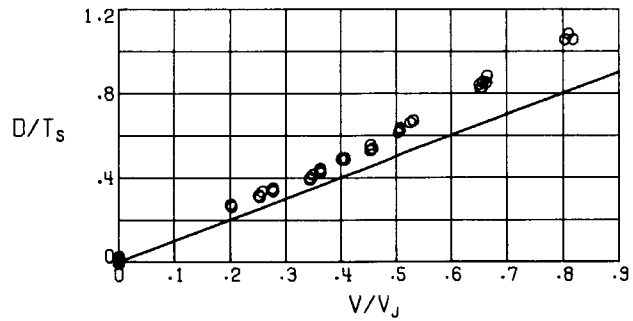


(e) $\alpha = 16^\circ$.

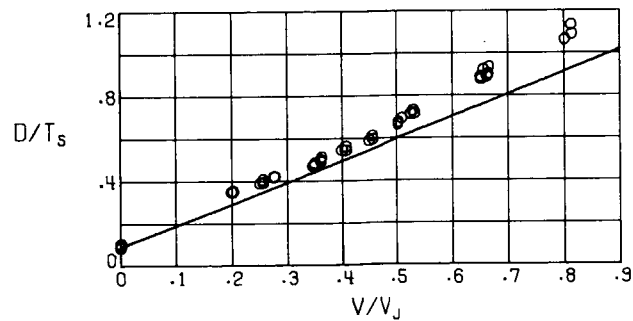
Figure 6.- Concluded.



(a) $\alpha = -5^\circ$.

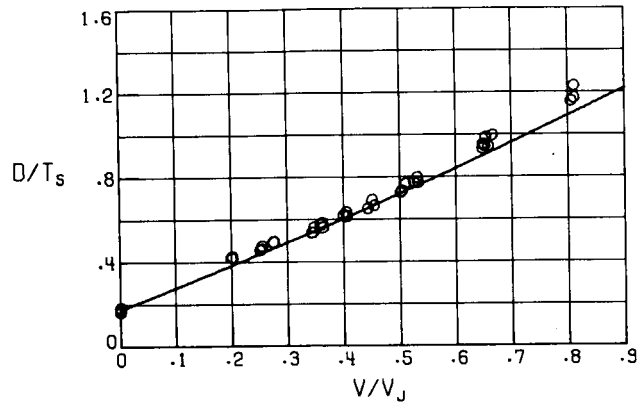


(b) $\alpha = 0^\circ$.

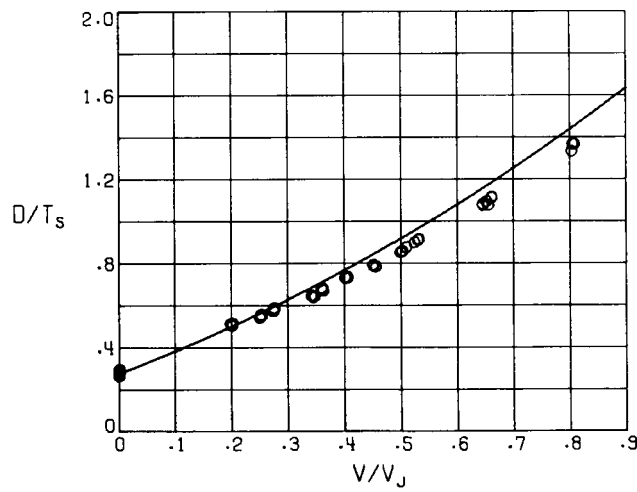


(c) $\alpha = 5^\circ$.

Figure 7.- Comparison of momentum theory with measurements of ratio of external drag to static thrust for a small fan-in-wing model tested in Langley full-scale wind tunnel. The theoretical curve is calculated from equation (55).

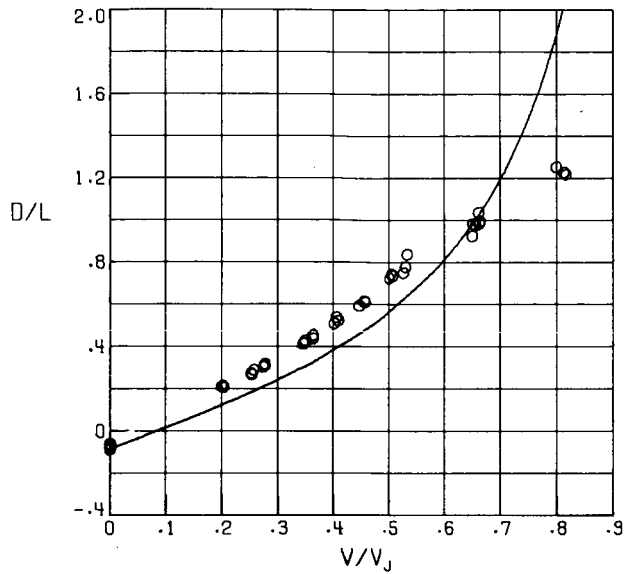


(d) $\alpha = 10^\circ$.

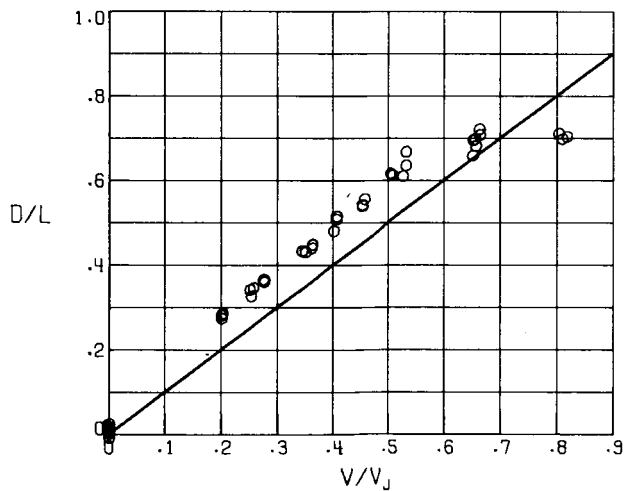


(e) $\alpha = 16^\circ$.

Figure 7.- Concluded.

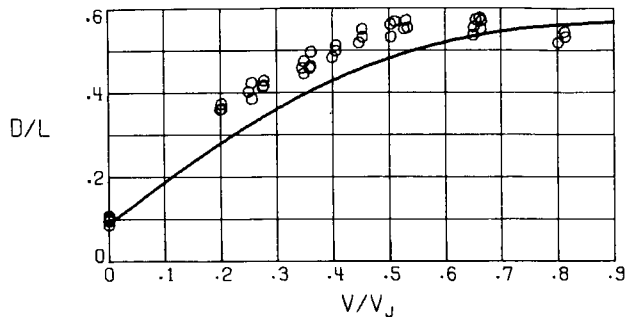


(a) $\alpha = -5^\circ$.

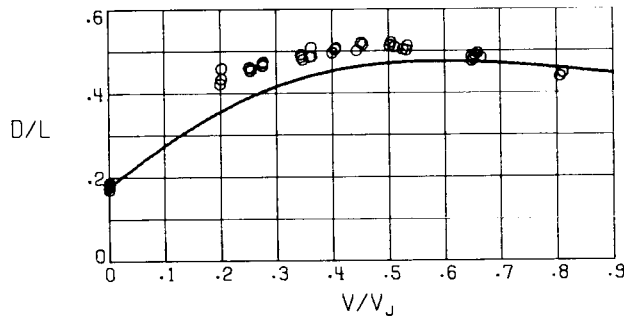


(b) $\alpha = 0^\circ$.

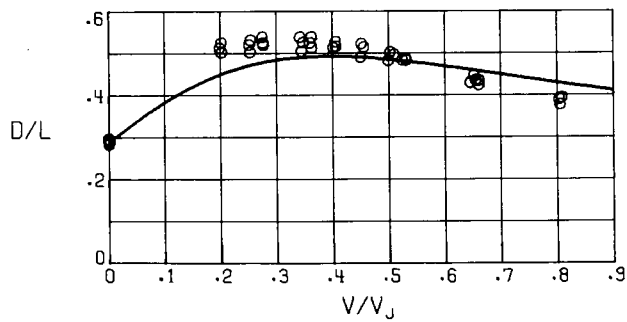
Figure 8.- Comparison of momentum theory with measurements of external drag-lift ratio for a small fan-in-wing model tested in Langley full-scale wind tunnel. The theoretical curve is calculated from equation (60).



(c) $\alpha = 5^\circ$.

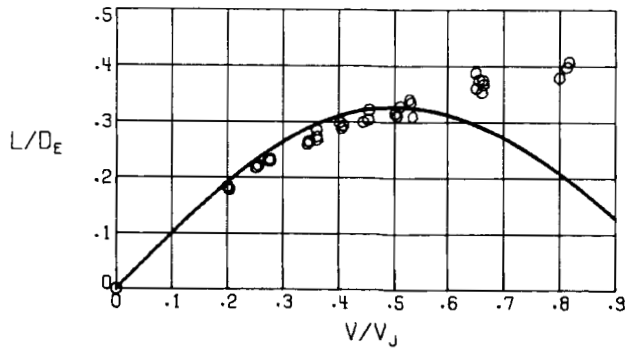


(d) $\alpha = 10^\circ$.

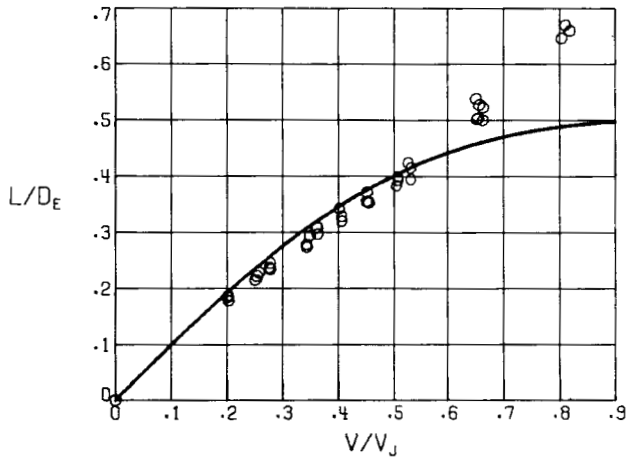


(e) $\alpha = 16^\circ$.

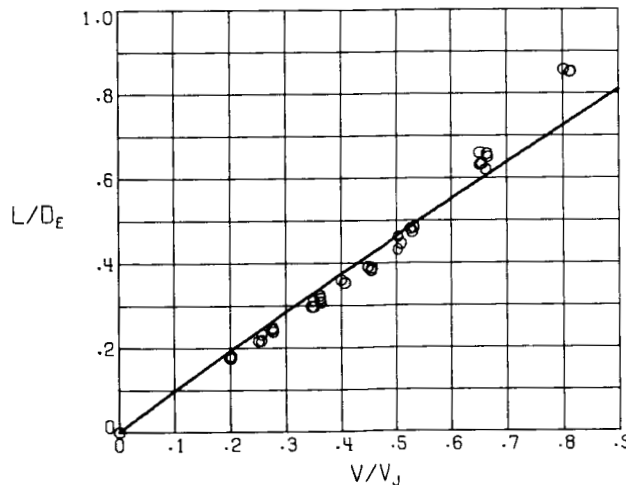
Figure 8.- Concluded.



(a) $\alpha = -5^\circ$.

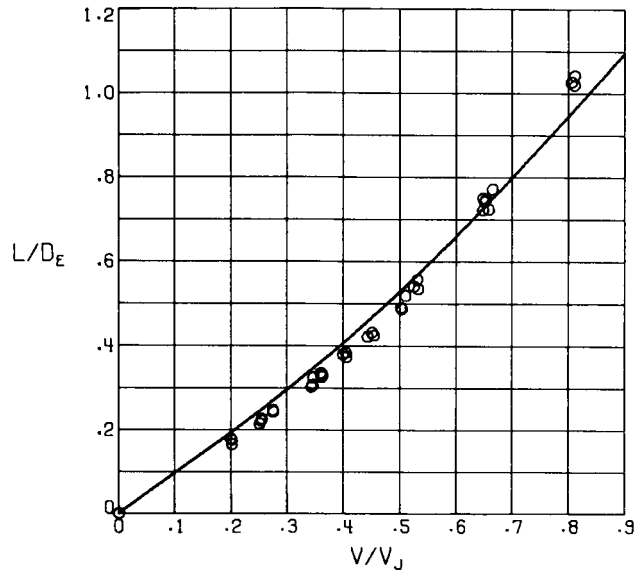


(b) $\alpha = 0^\circ$.

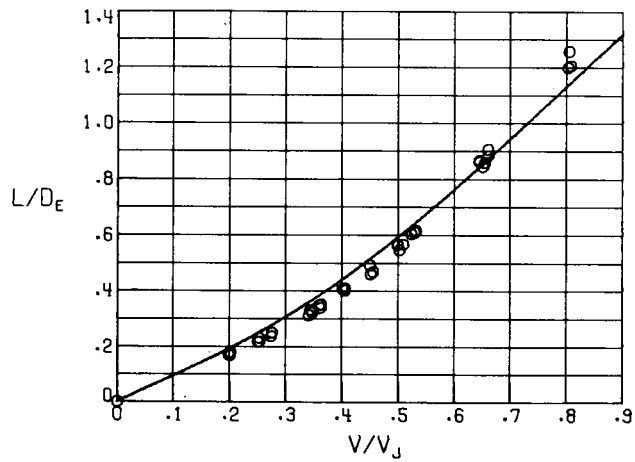


(c) $\alpha = 5^\circ$.

Figure 9.- Comparison of momentum theory with measurements of equivalent lift-drag ratio for a small fan-in-wing model tested in Langley full-scale wind tunnel. A drag equivalent to ideal fan power (eq. (67)) has been added to the experimental data. The theoretical curve has been calculated from equations (63) and (65).



(d) $\alpha = 10^\circ$.



(e) $\alpha = 16^\circ$.

Figure 9.- Concluded.

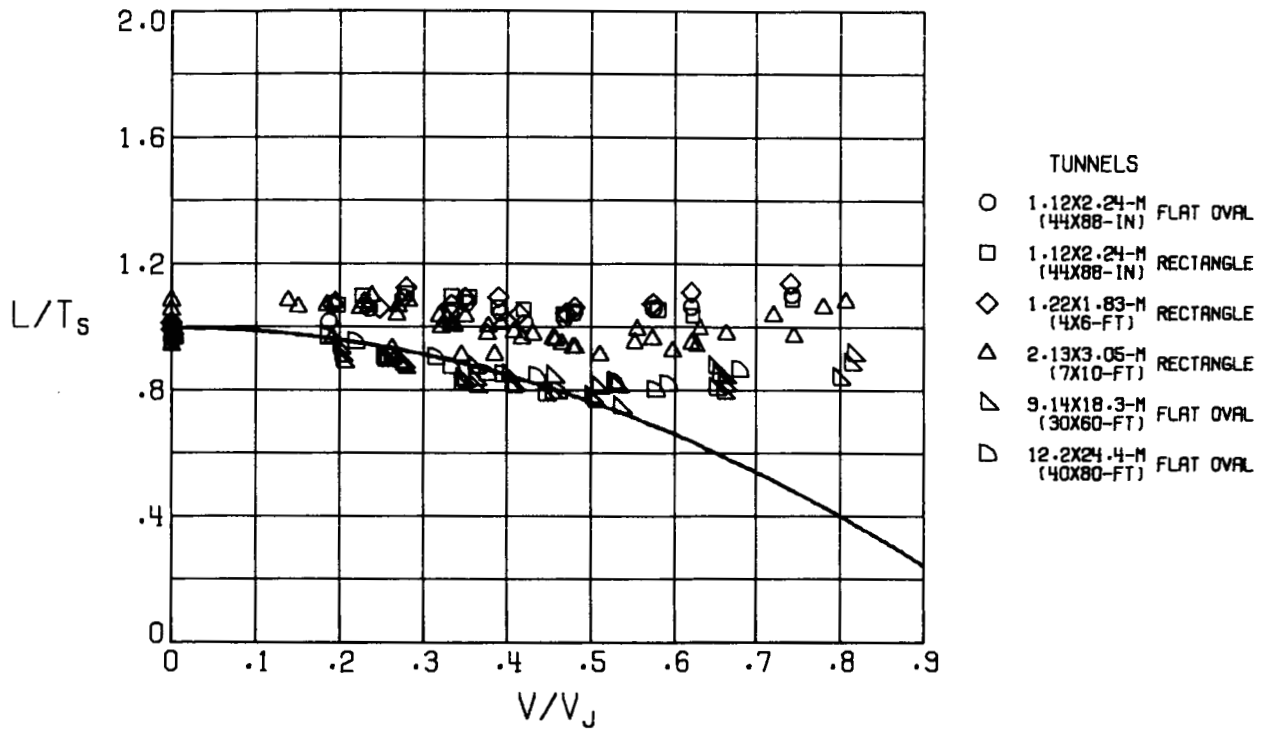
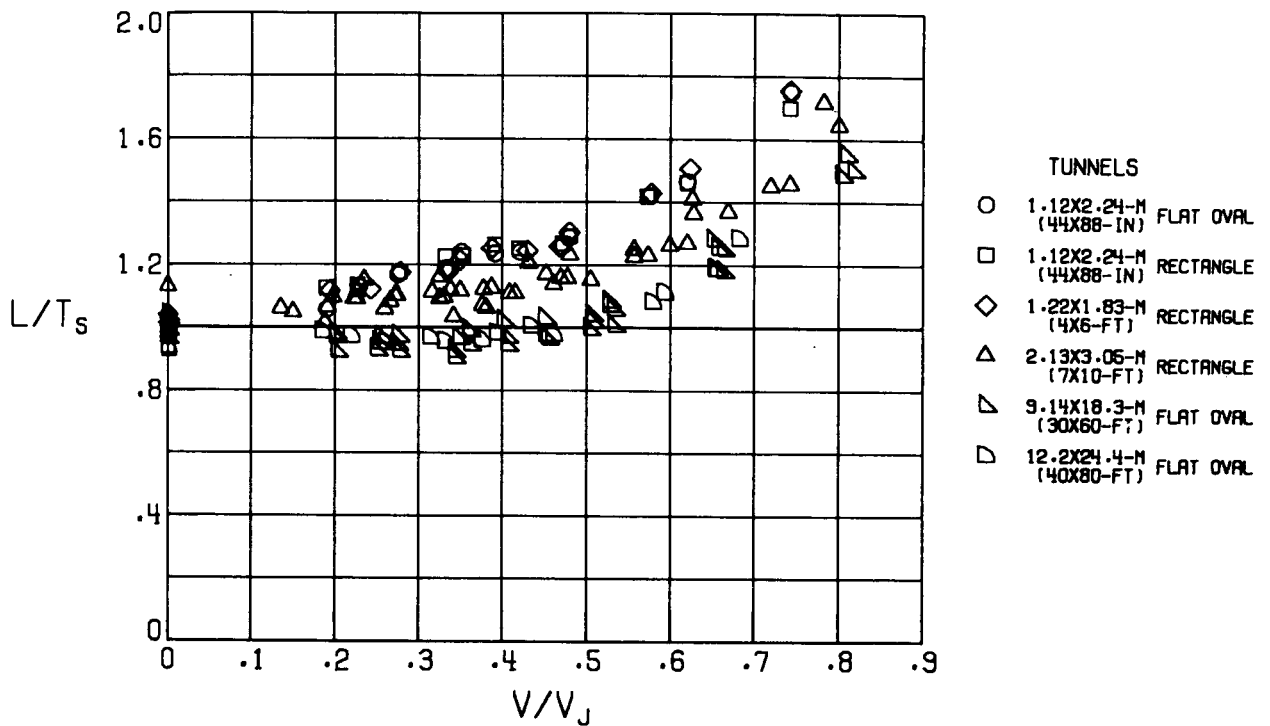
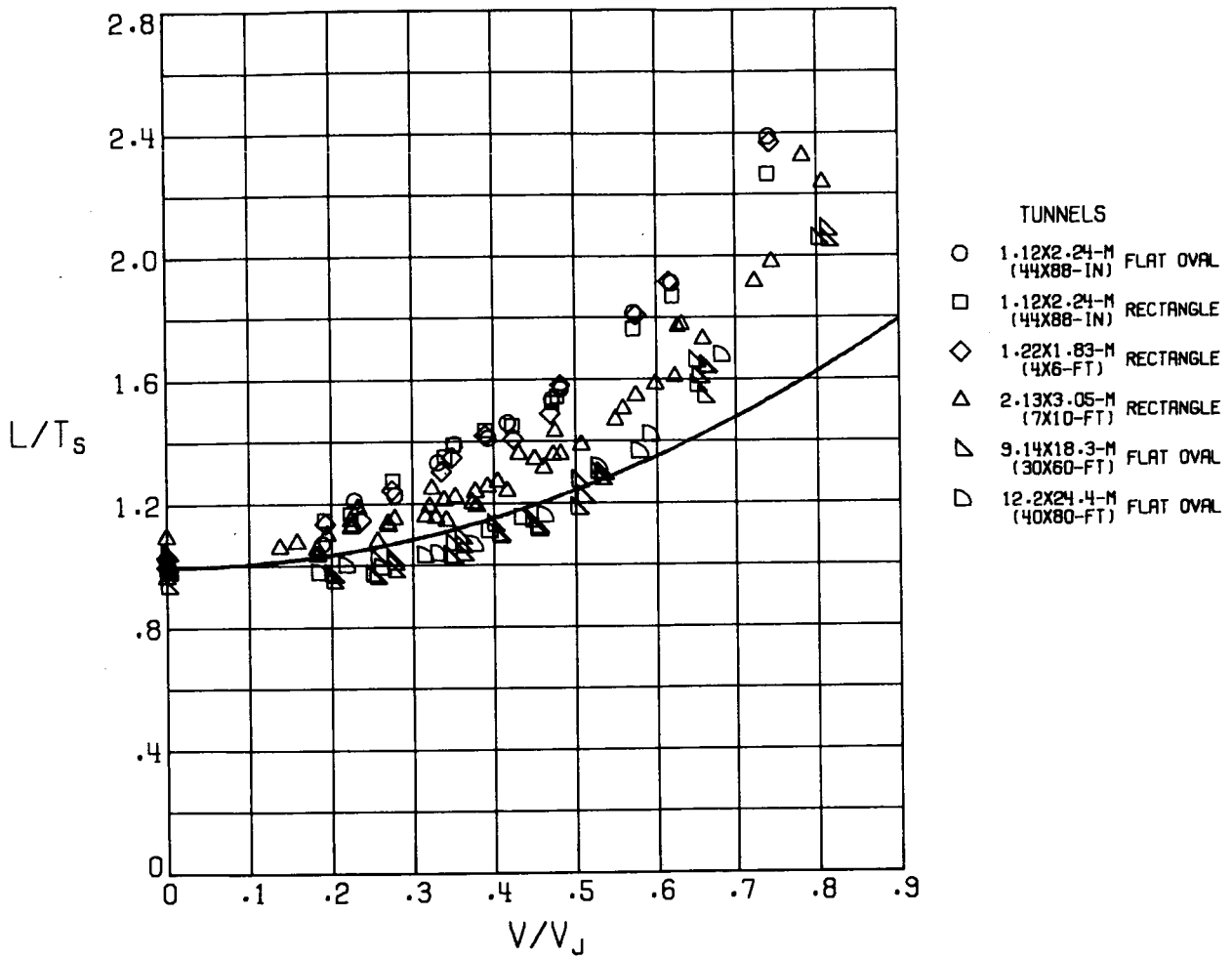


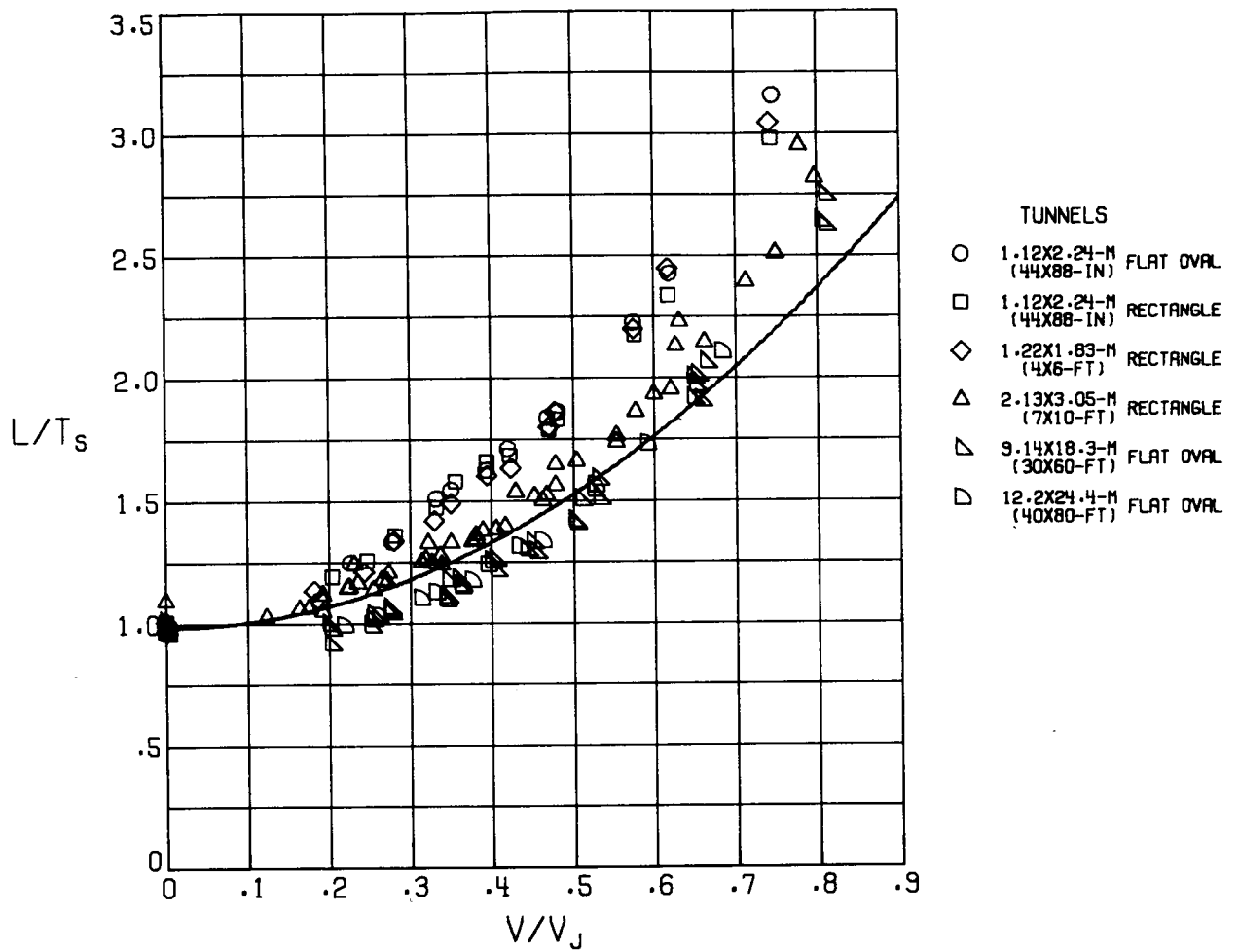
Figure 10.- Uncorrected values of ratio of lift to static thrust as measured in several test sections of differing cross-sectional area. The theoretical curve is calculated from equation (54). (Reproduced from ref. 15.)



(b) $\alpha = 0^\circ$.

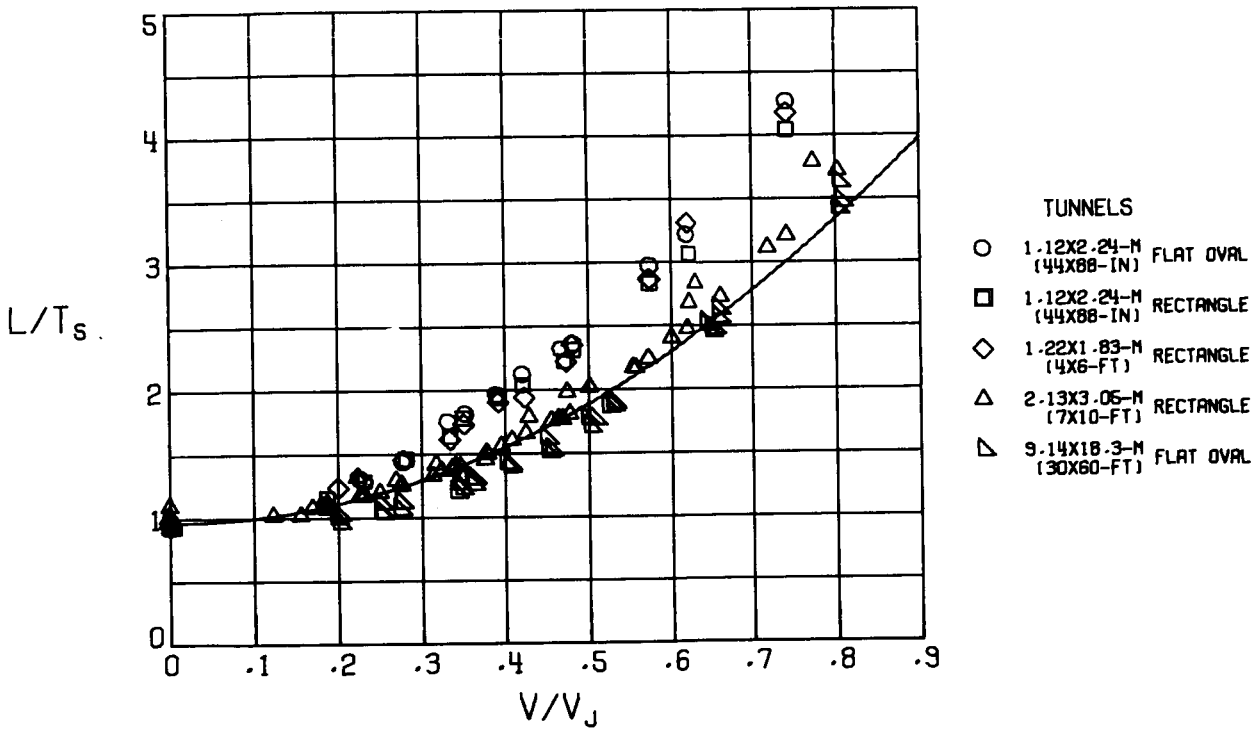
Figure 10.- Continued.





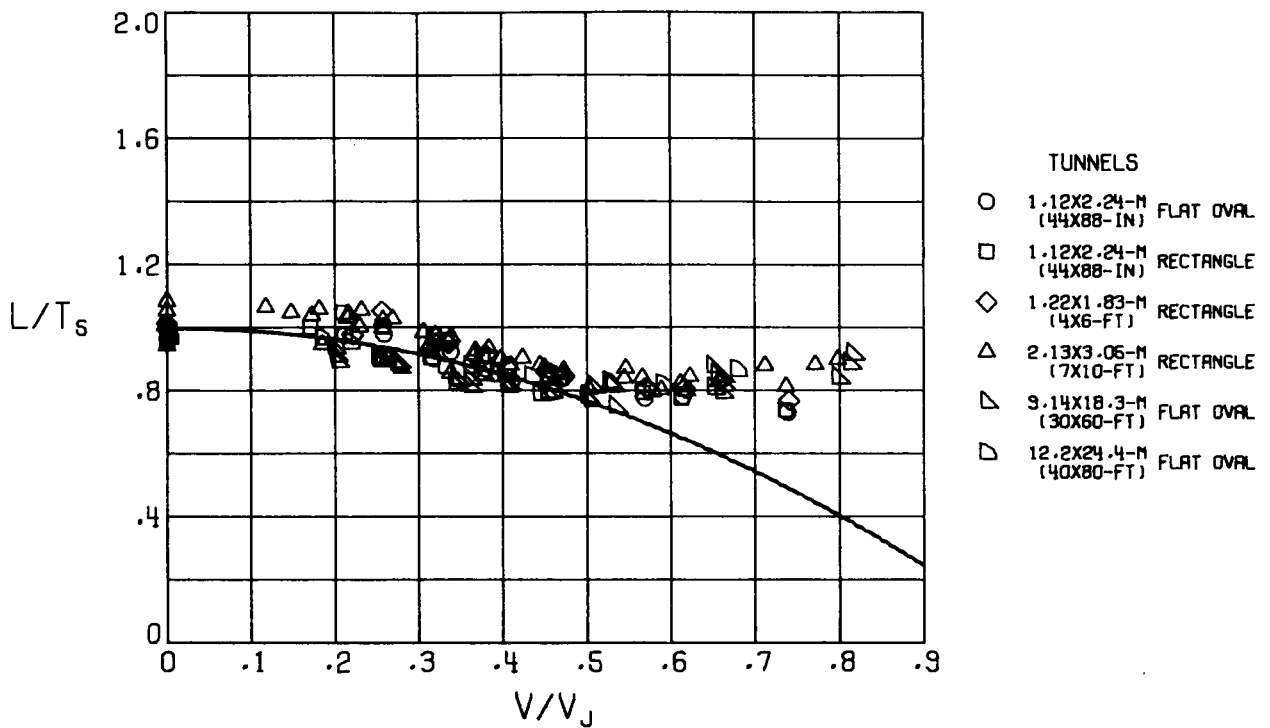
(d) $\alpha = 10^\circ$.

Figure 10.- Continued.



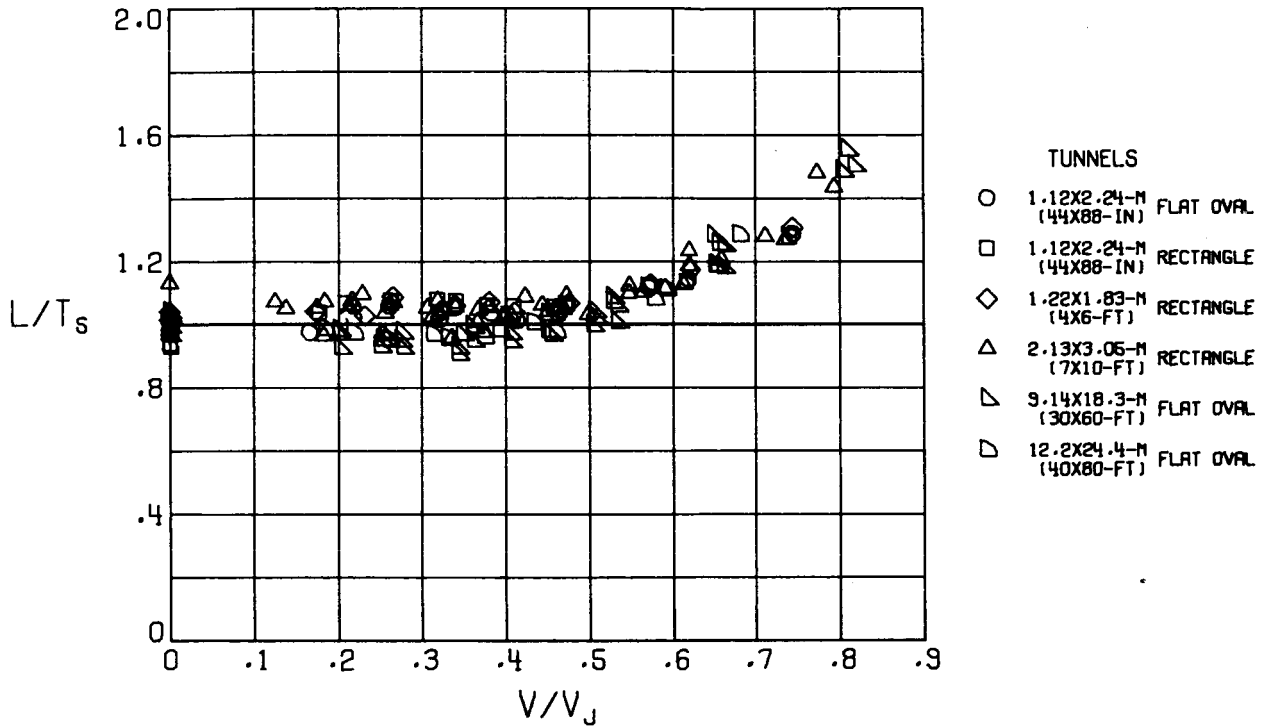
(e) $\alpha = 16^\circ$.

Figure 10.- Concluded.



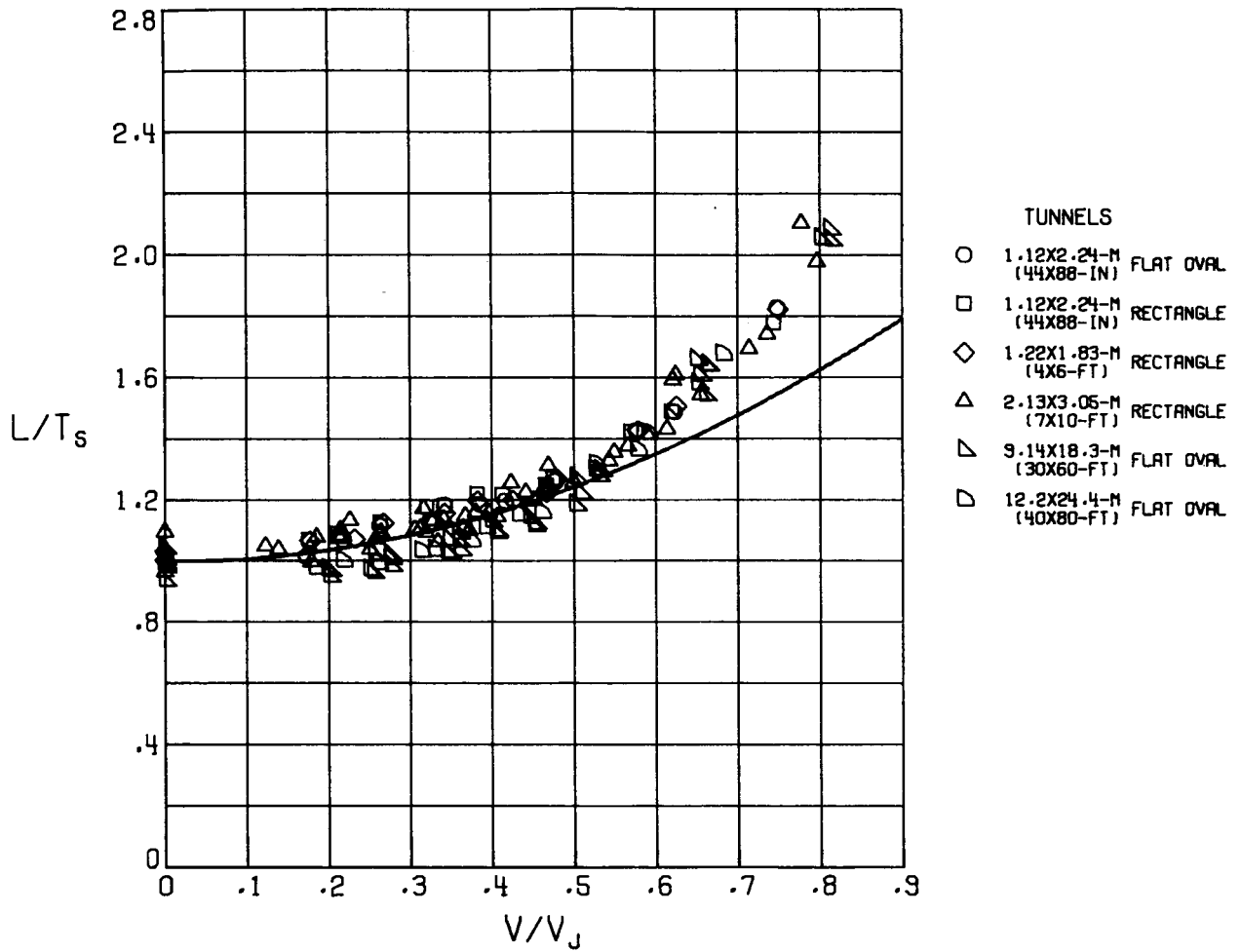
(a) $\alpha = -5^\circ$.

Figure 11.- Corrected values of ratio of lift to static thrust as measured in several test sections of differing cross-sectional area. The theoretical curve is calculated from equation (54). (Reproduced from ref. 15.)



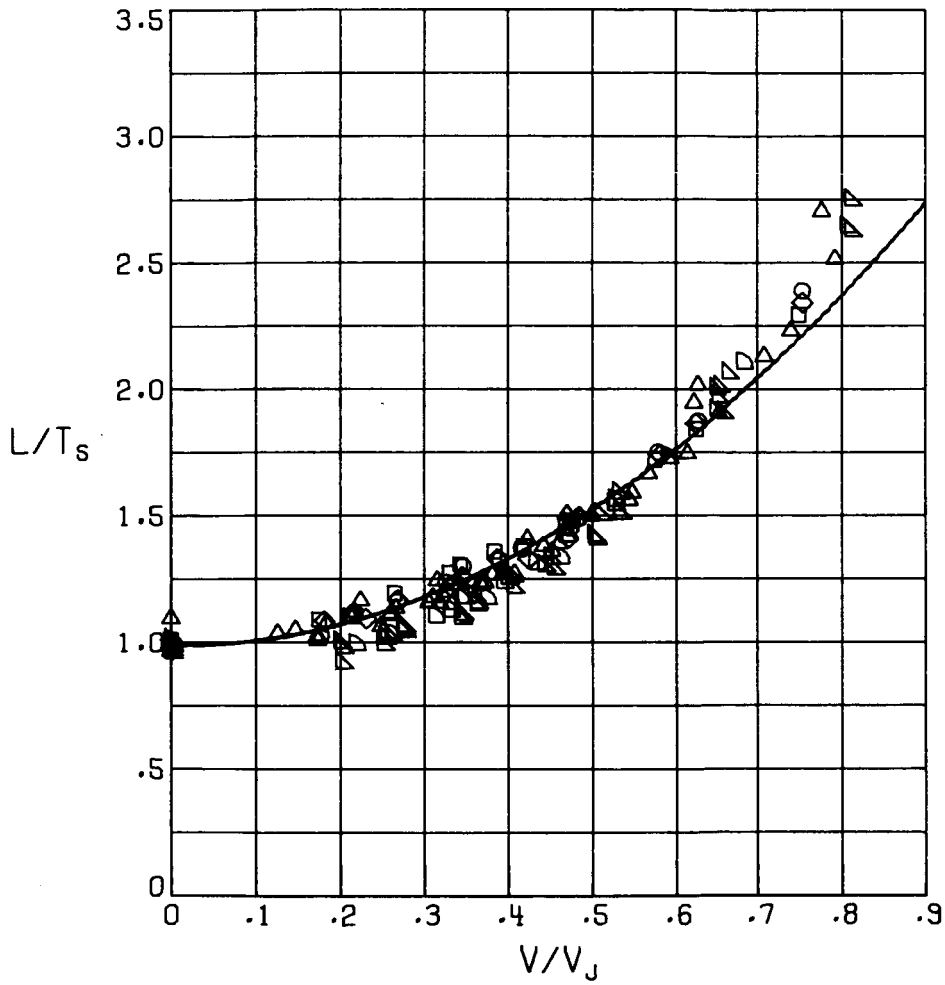
(b) $\alpha = 0^\circ$.

Figure 11.- Continued.



(c) $\alpha = 5^\circ$.

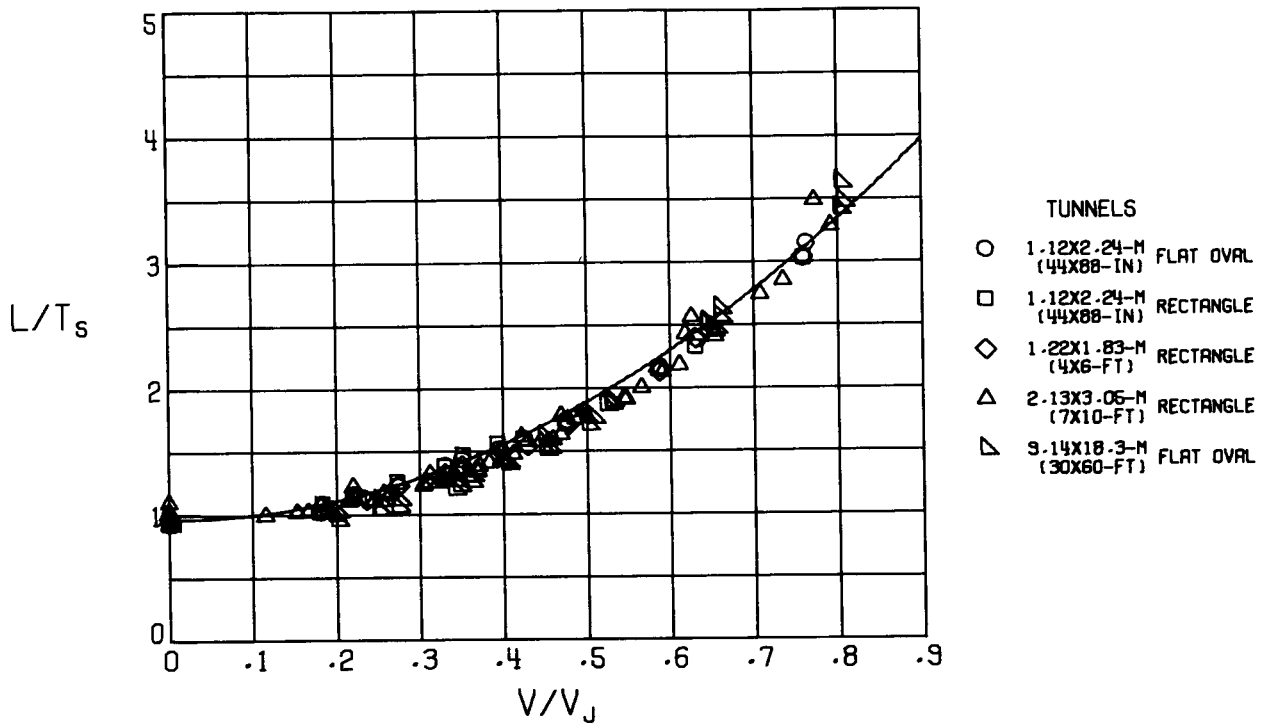
Figure 11.- Continued.



- TUNNELS
- 1.12X2.24-M (44X88-IN) FLAT OVAL
 - 1.12X2.24-M (44X88-IN) RECTANGLE
 - ◇ 1.22X1.83-M (4X6-FT) RECTANGLE
 - △ 2.13X3.05-M (7X10-FT) RECTANGLE
 - ▽ 9.14X18.3-M (30X60-FT) FLAT OVAL
 - ◁ 12.2X24.4-M (40X80-FT) FLAT OVAL

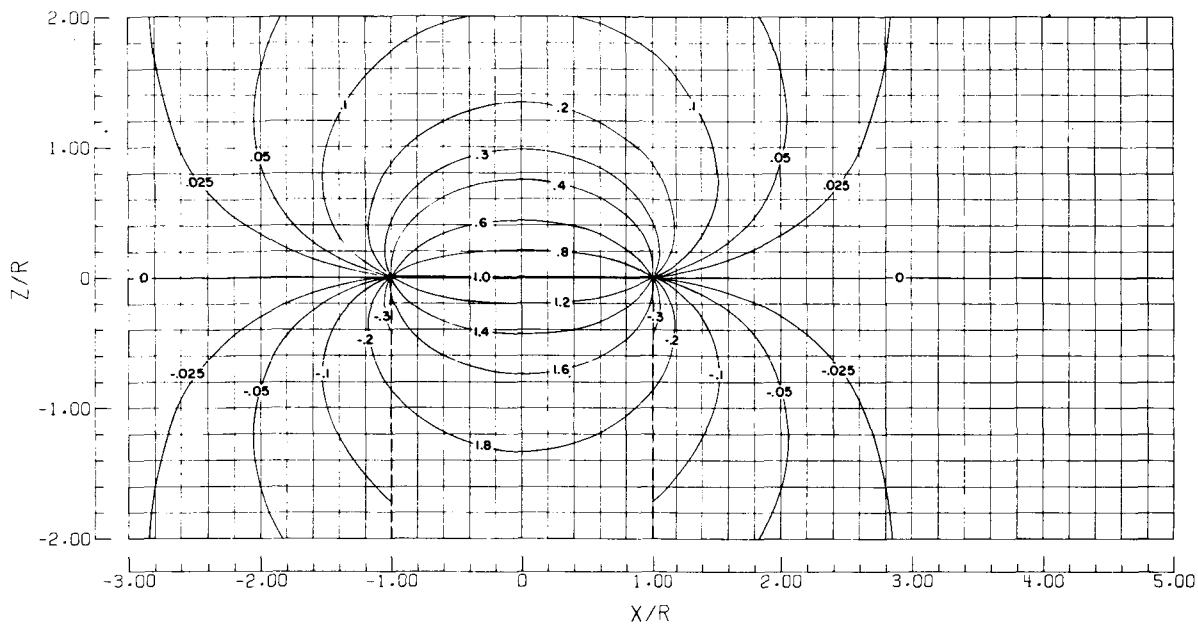
(d) $\alpha = 10^\circ$.

Figure 11.- Continued.

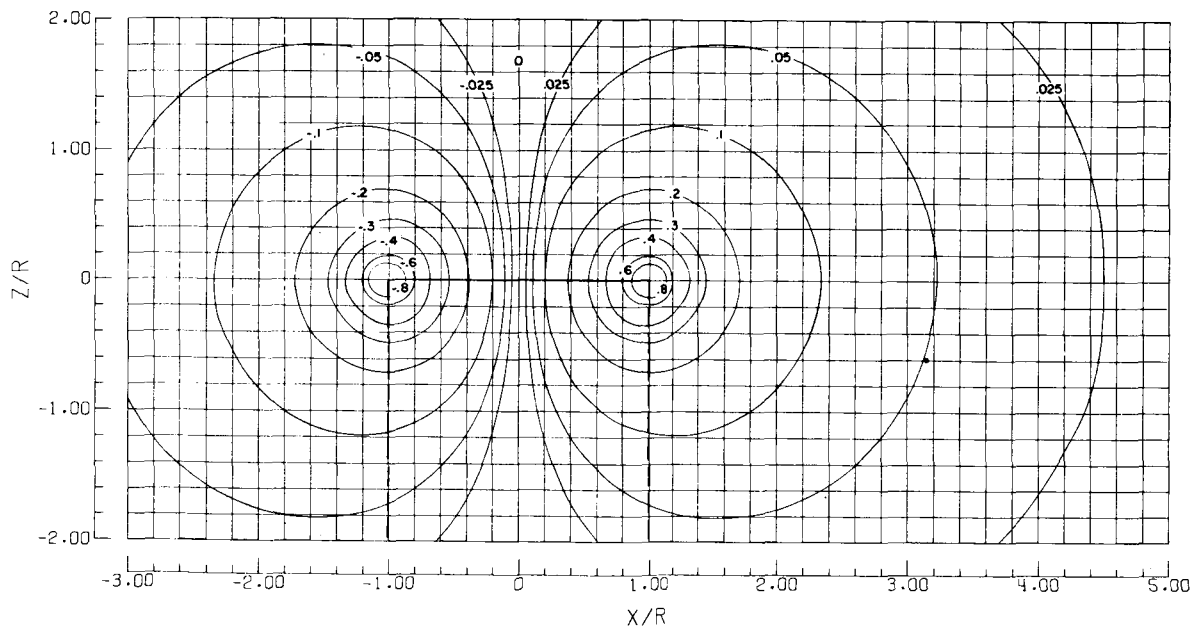


(e) $\alpha = 16^\circ$.

Figure 11.- Concluded.



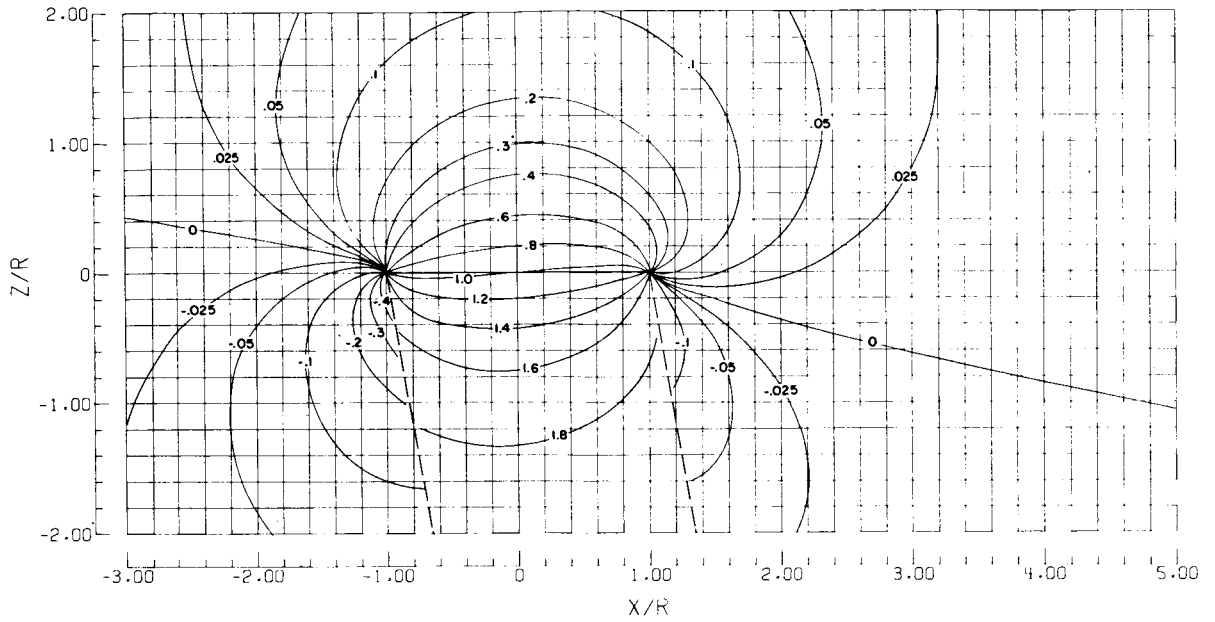
Contours of w/w_0



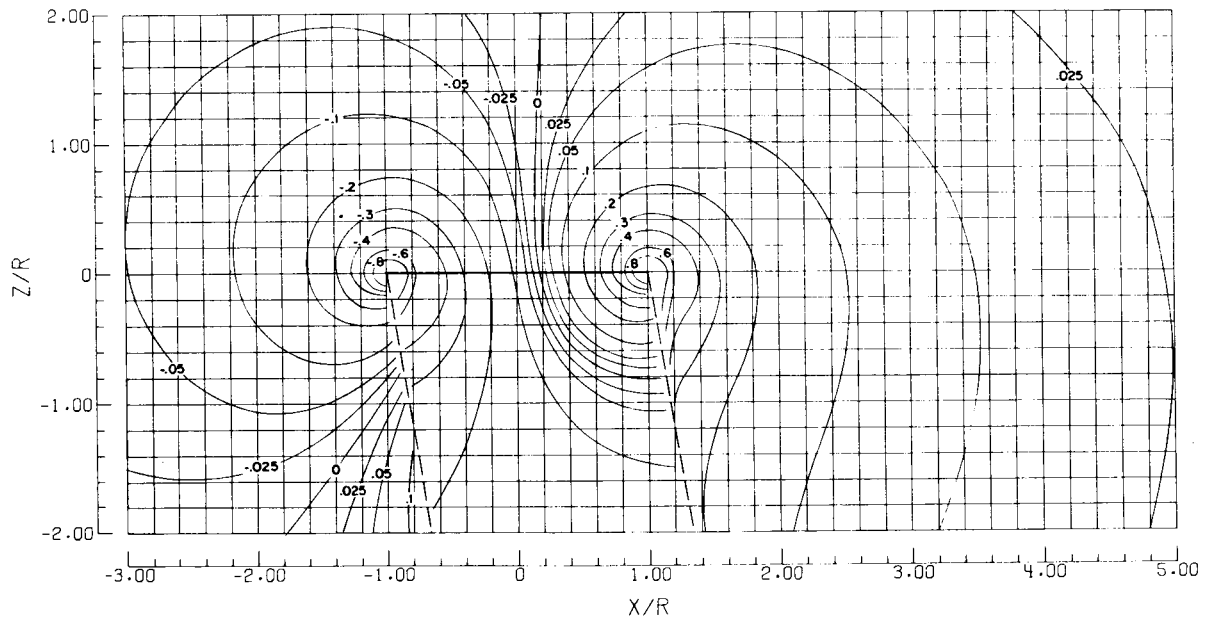
Contours of u/w_0

(a) $\chi = 0^\circ$.

Figure 12.- Induced velocity ratios in center plane of a rotor with uniform disk-load distribution.



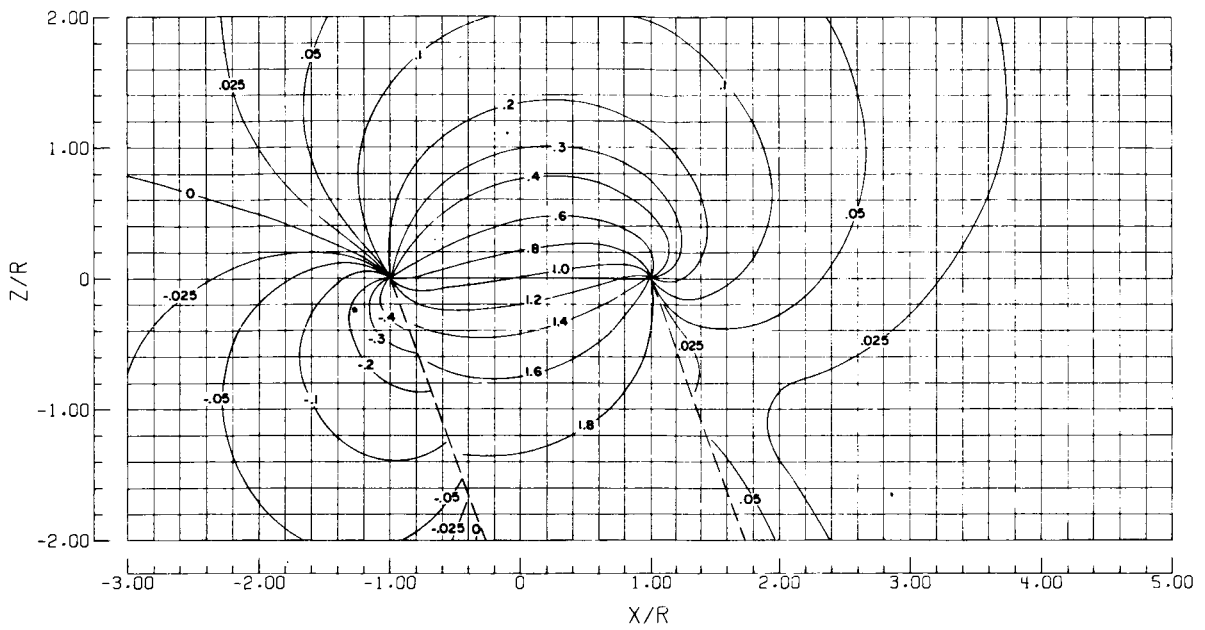
Contours of w/w_0



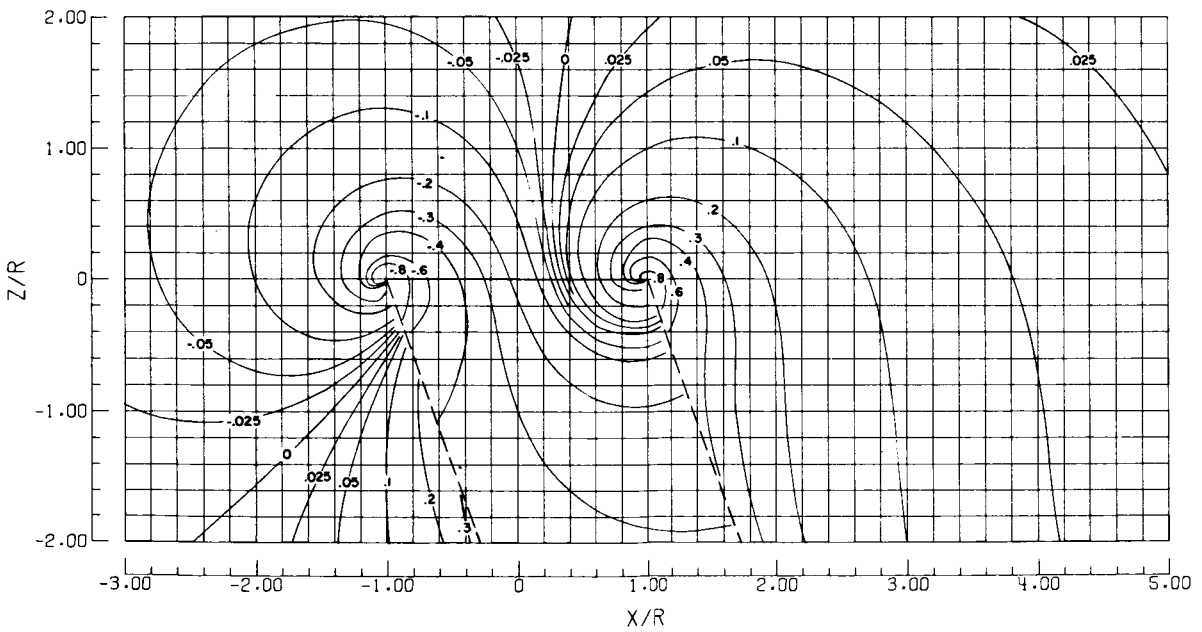
Contours of u/w_0

(b) $\chi = 10^\circ$.

Figure 12.- Continued.



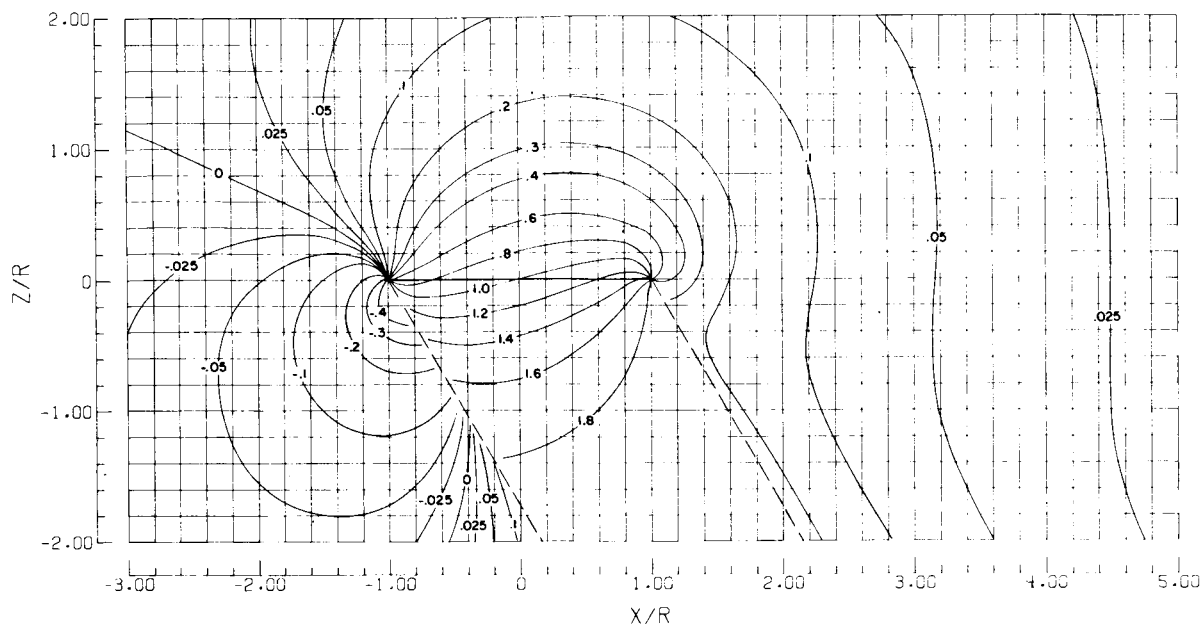
Contours of w/w_0



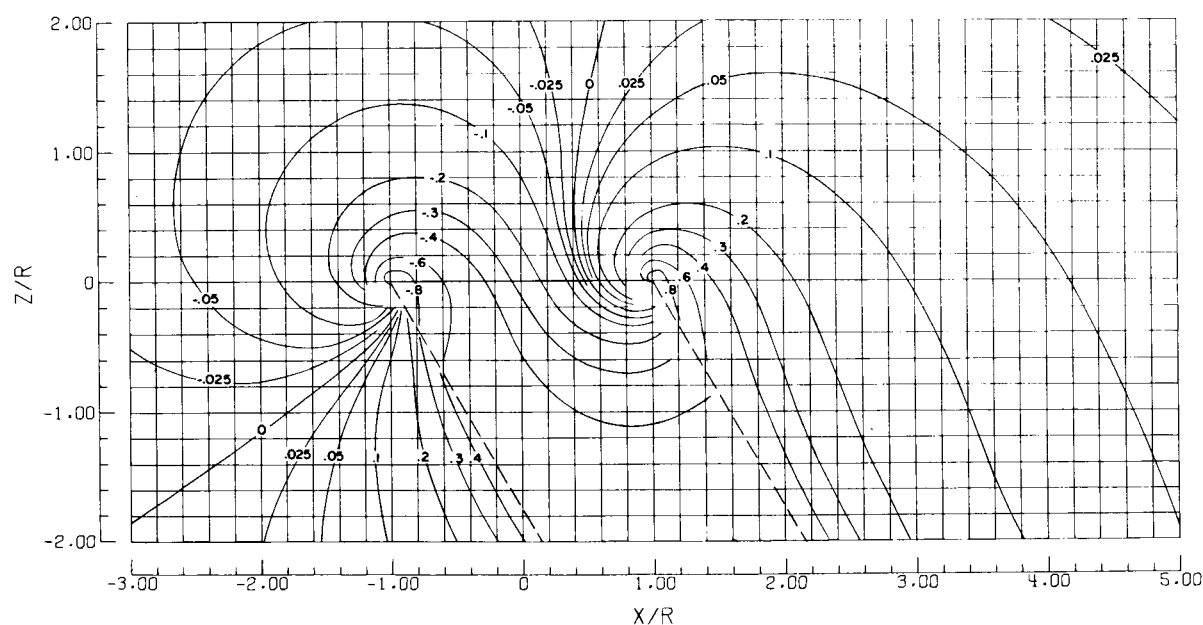
Contours of u/w_0

(c) $\chi = 20^\circ$.

Figure 12.- Continued.



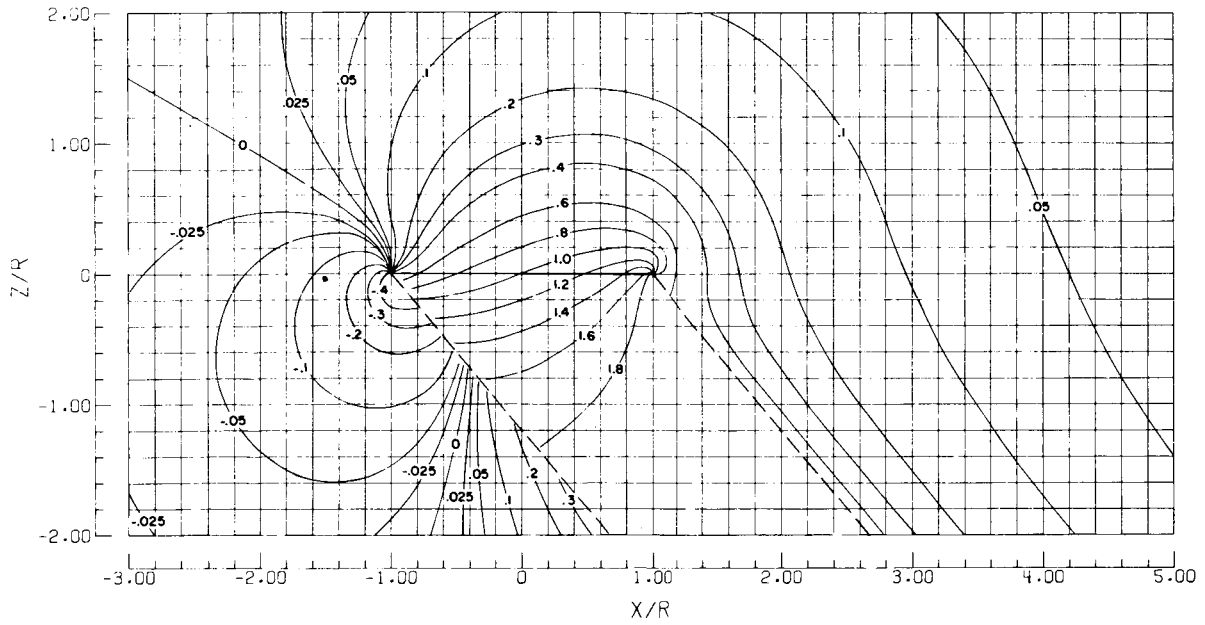
Contours of w/w_0



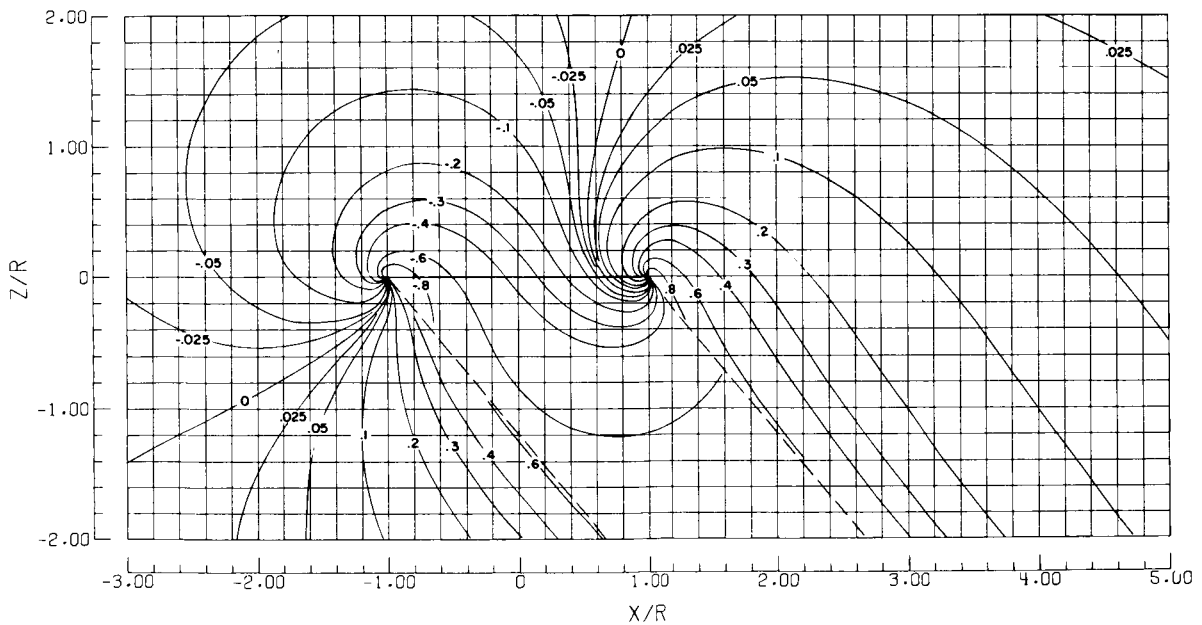
Contours of u/w_0

(d) $\chi = 30^\circ$.

Figure 12.- Continued.



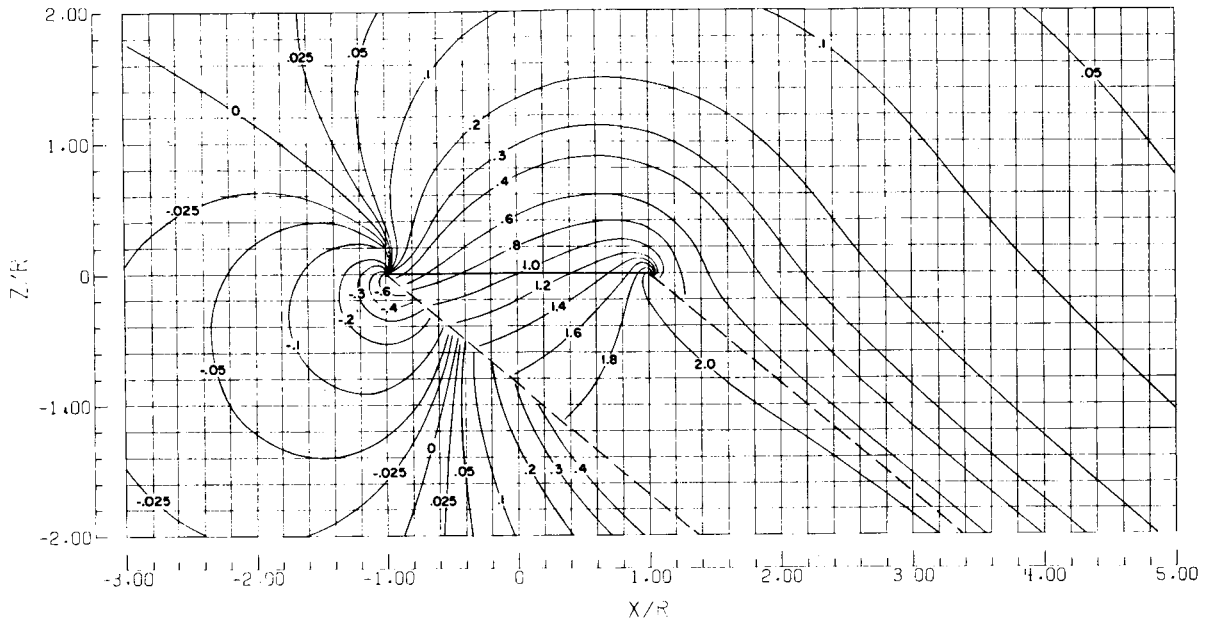
Contours of w/w_0



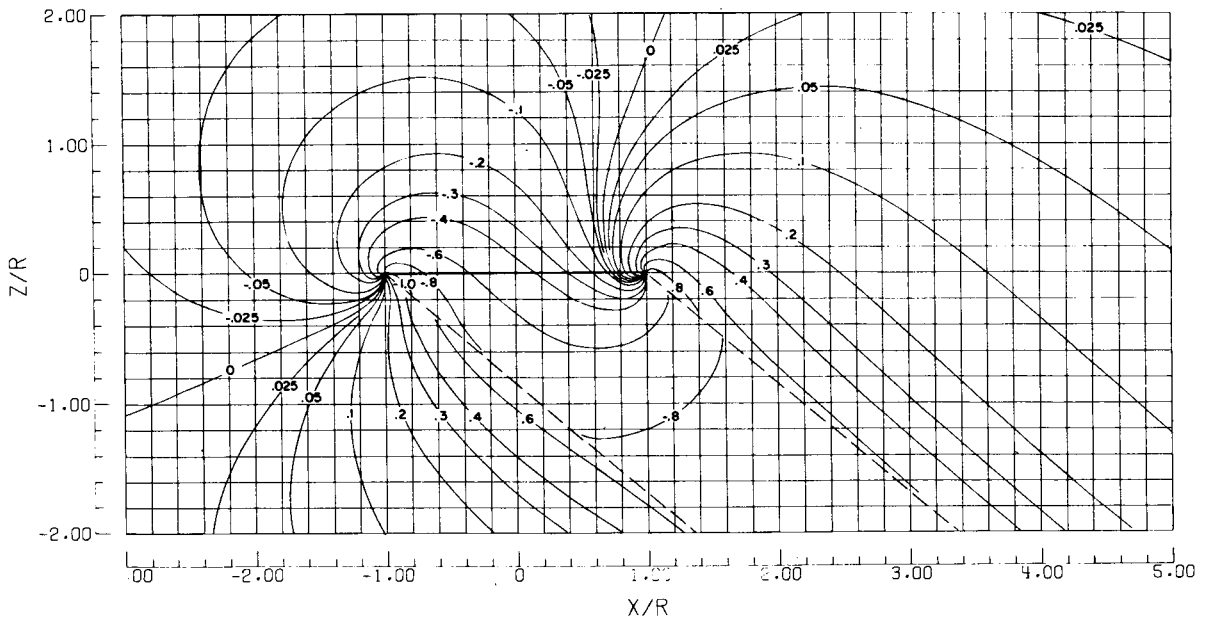
Contours of u/w_0

(e) $\chi = 40^\circ$.

Figure 12.- Continued.



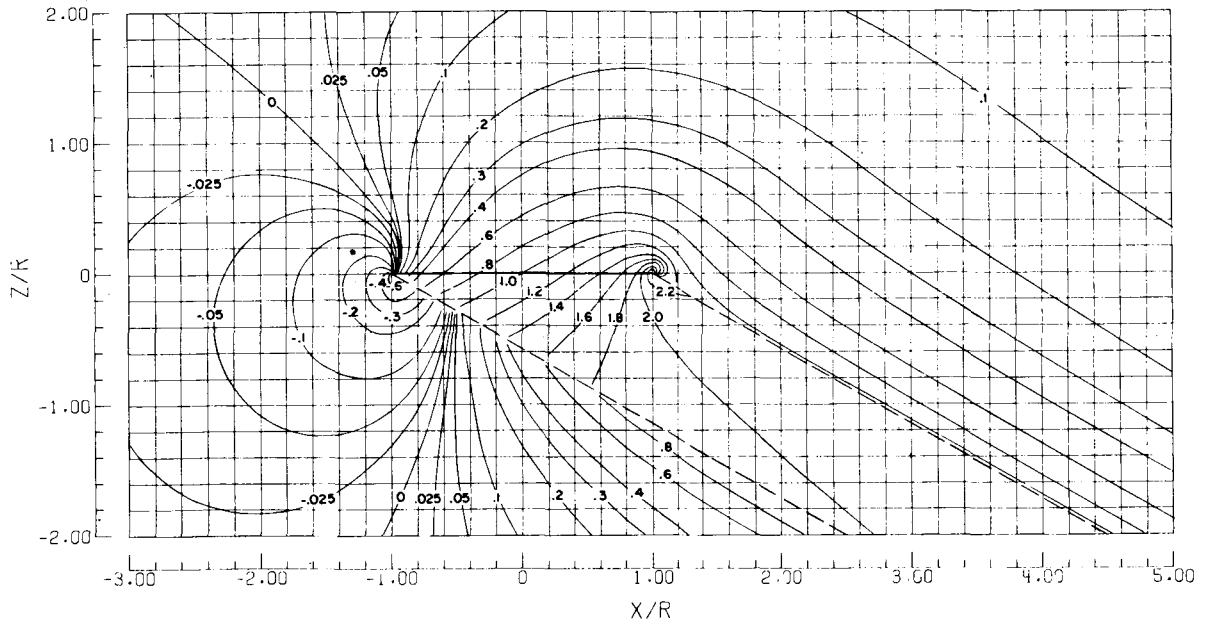
Contours of w/w_0



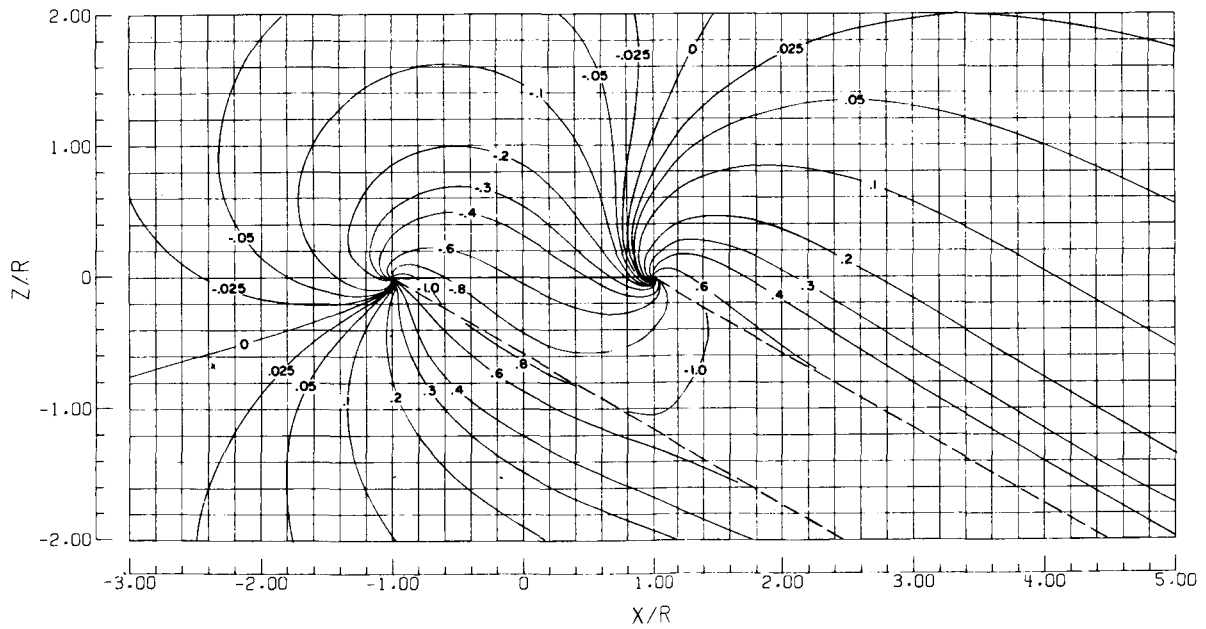
Contours of u/w_0

(f) $\chi = 50^\circ$.

Figure 12.- Continued.



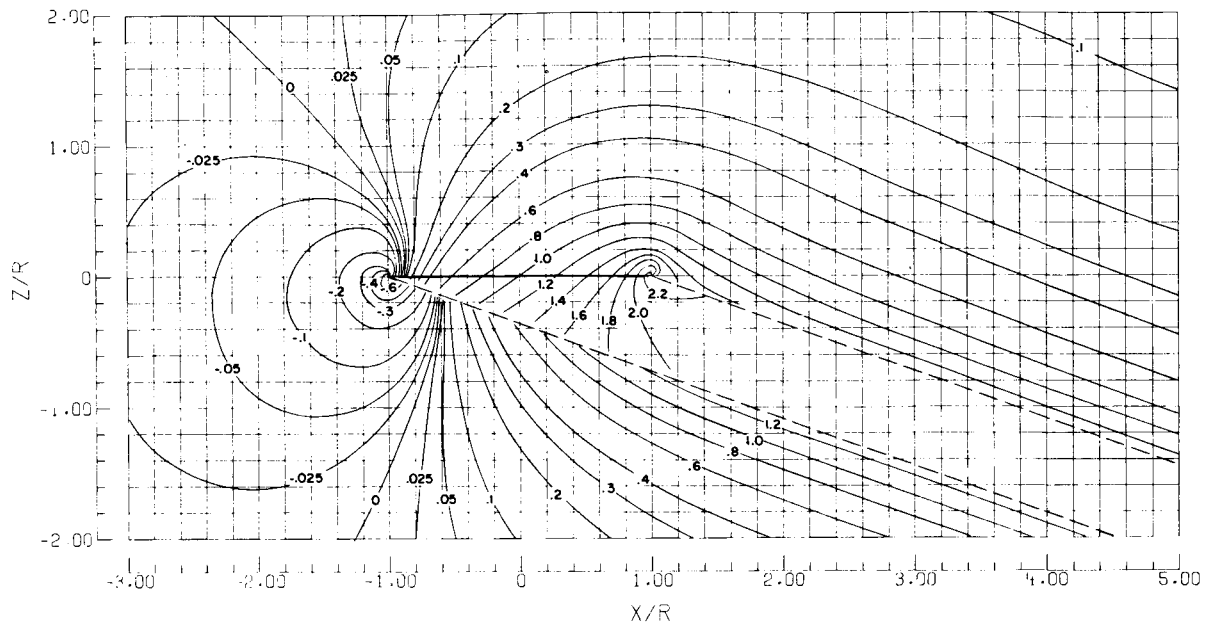
Contours of w/w_0



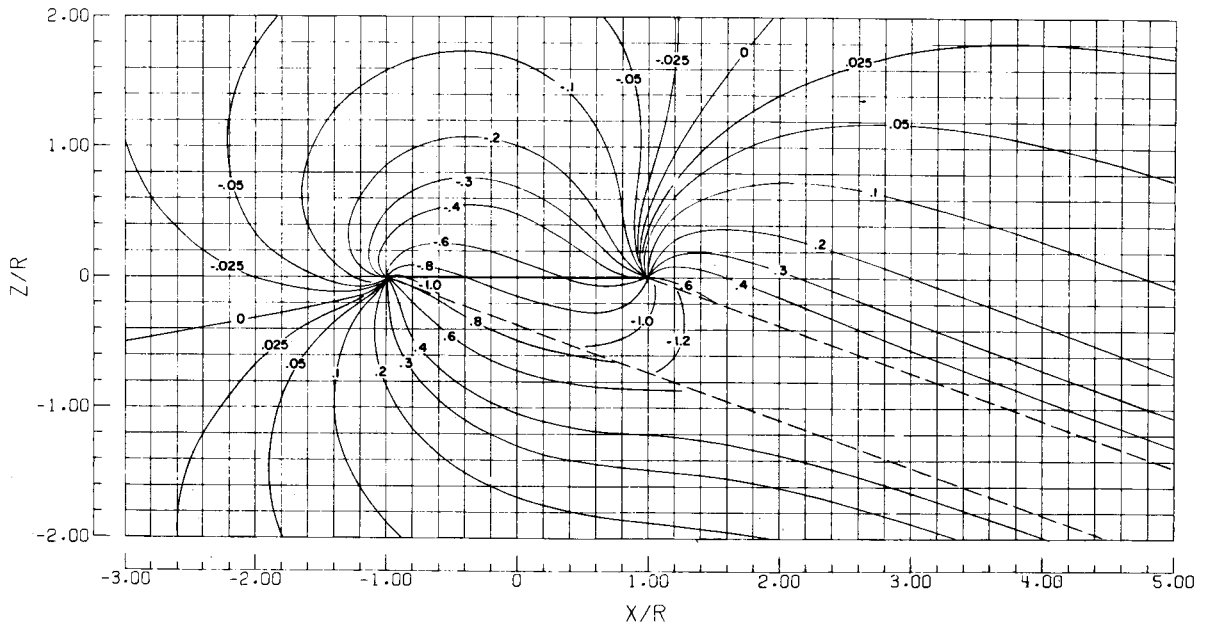
Contours of u/w_0

(g) $\chi = 60^\circ$.

Figure 12.- Continued.



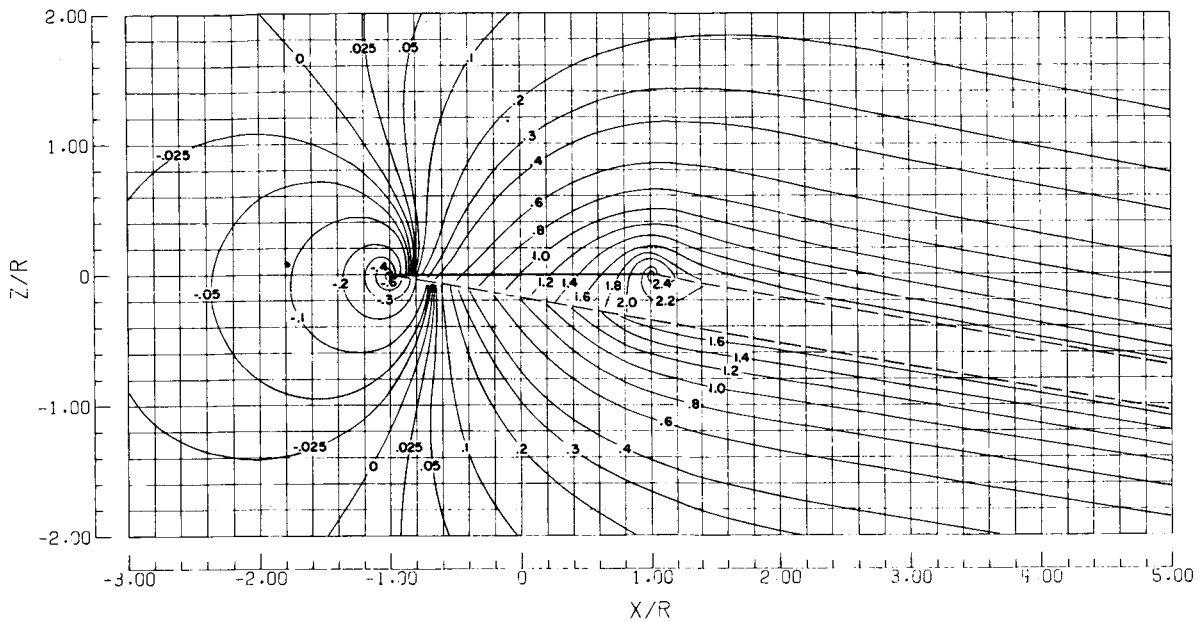
Contours of w/w_0



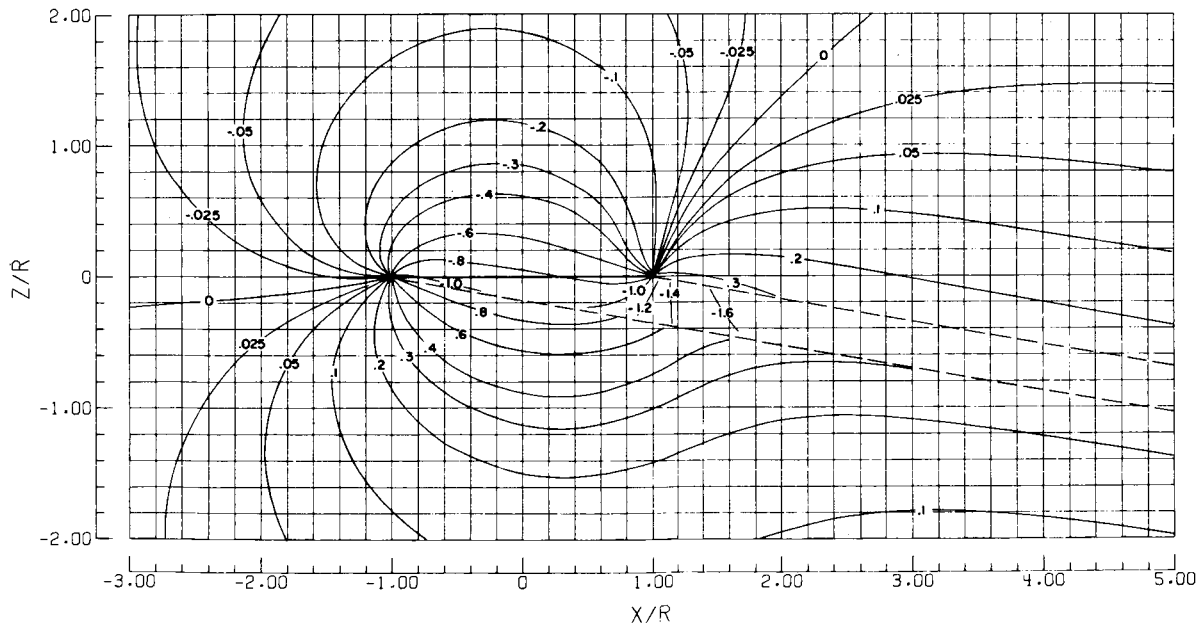
Contours of u/w_0

(h) $\chi = 70^\circ$.

Figure 12.- Continued.



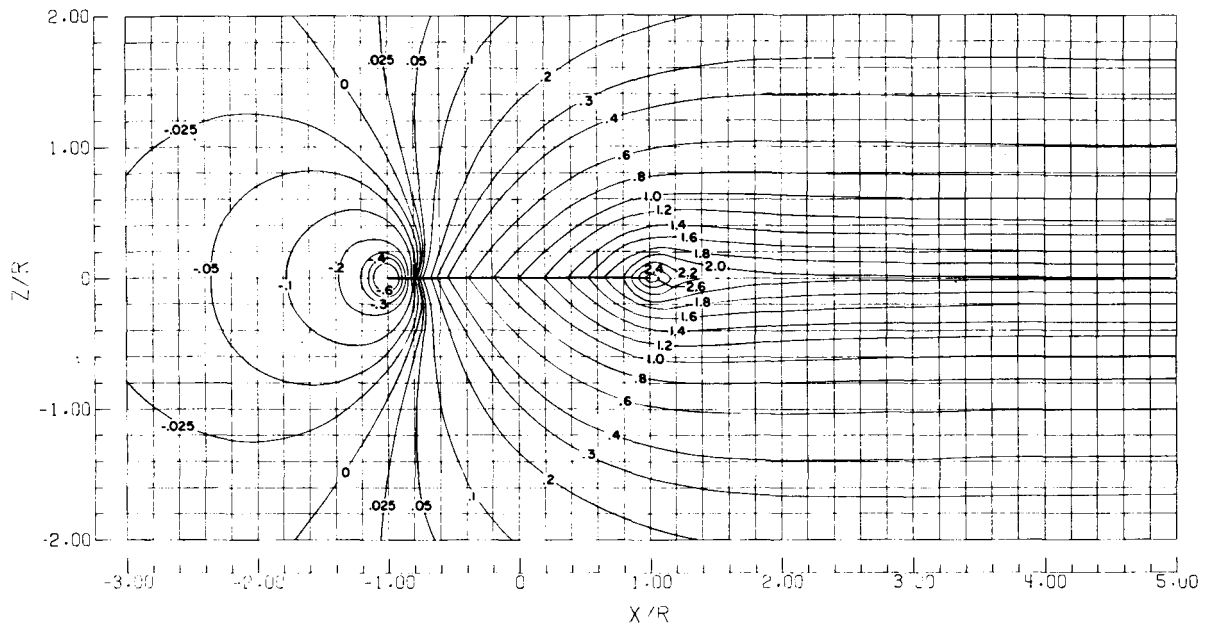
Contours of w/w_0



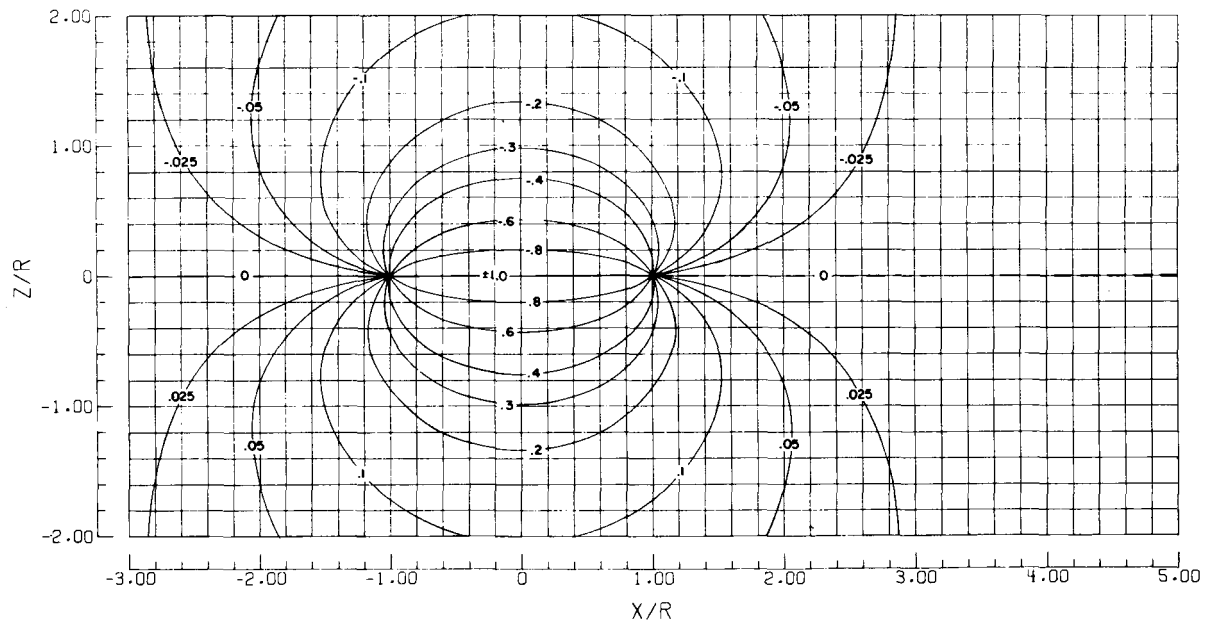
Contours of u/w_0

(i) $\chi = 80^\circ$.

Figure 12.- Continued.



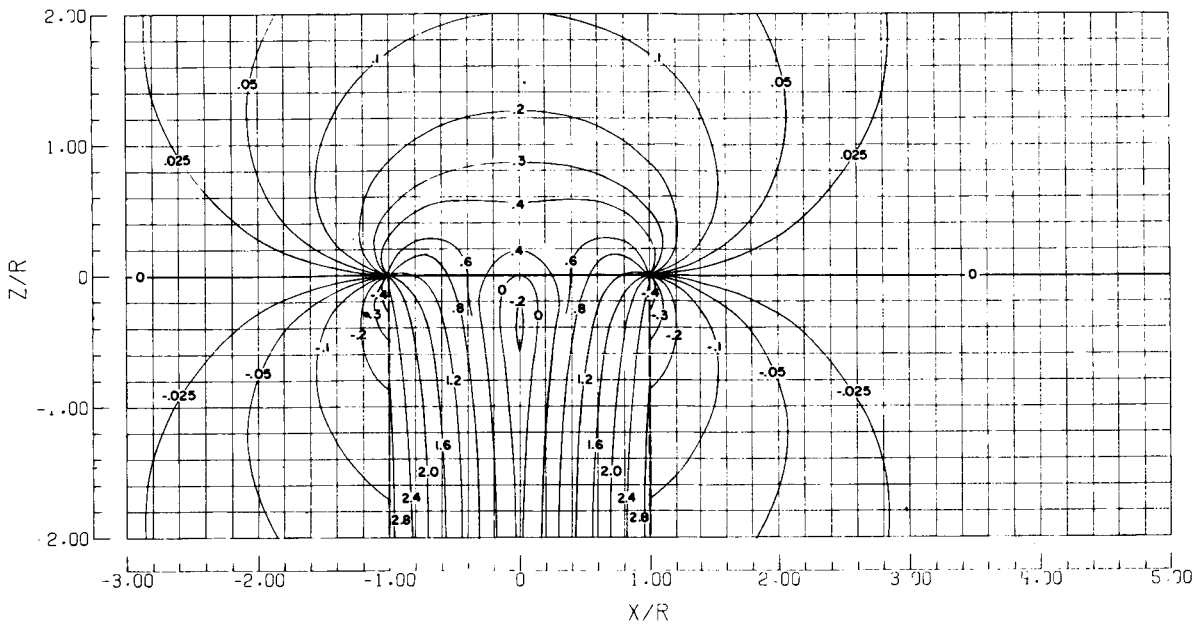
Contours of w/w_0



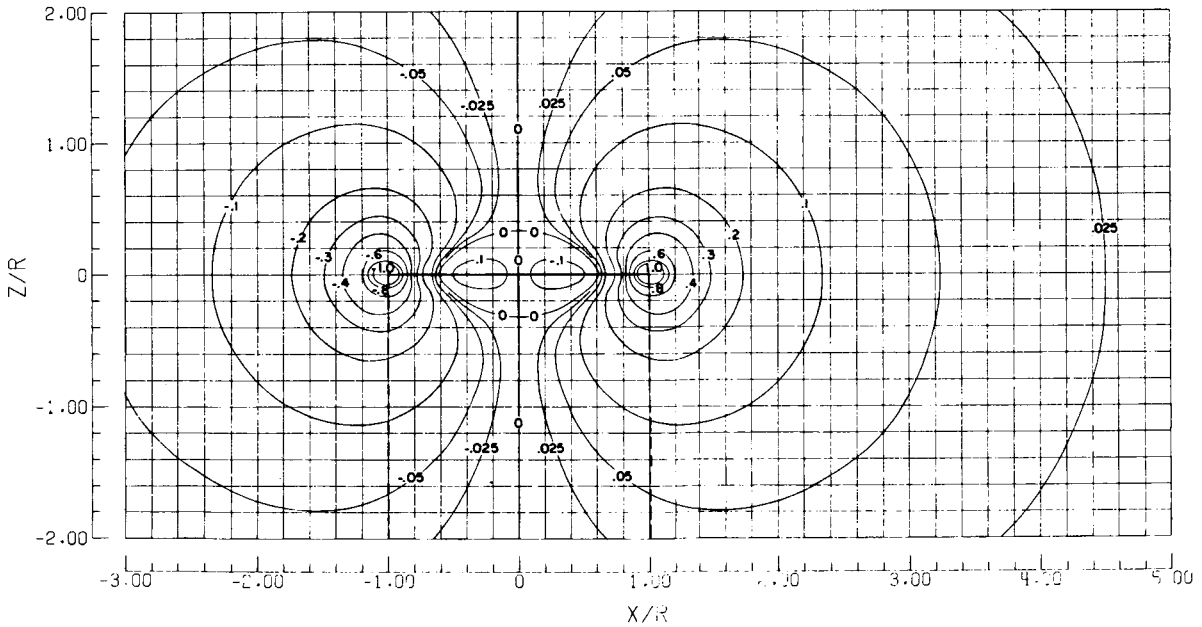
Contours of u/w_0

(j) $\chi = 90^\circ$.

Figure 12.- Concluded.



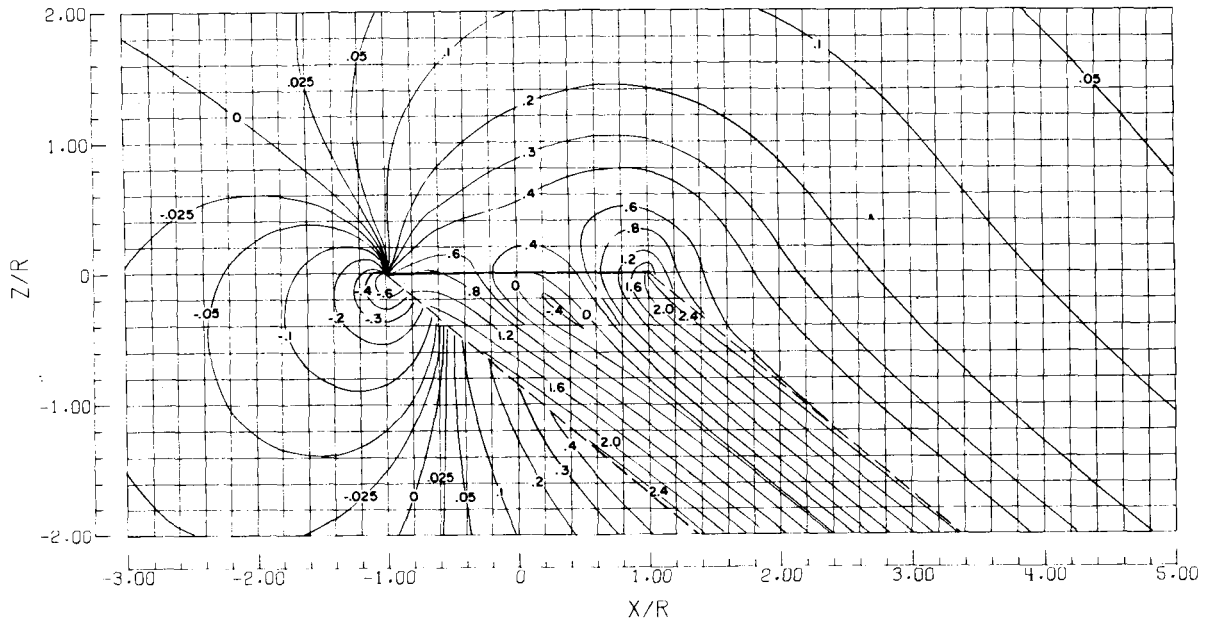
Contours of w/w_0



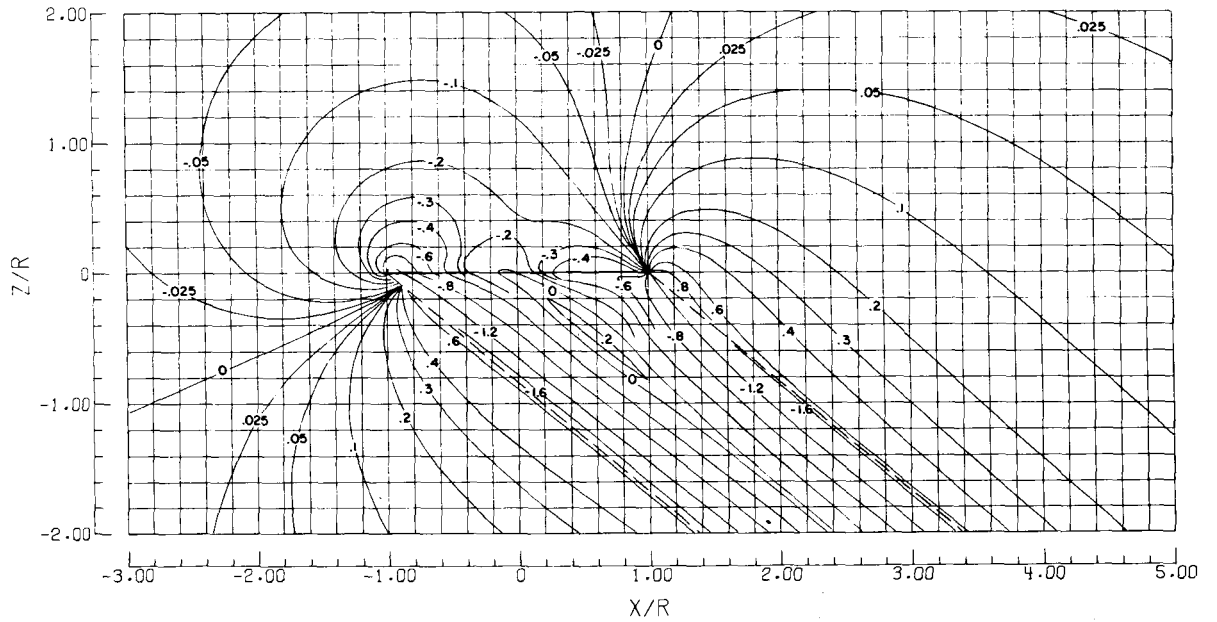
Contours of u/w_0

(a) $\chi = 0^\circ$.

Figure 13.- Induced velocity ratios in center plane of a rotor with triangular disk-load distribution.



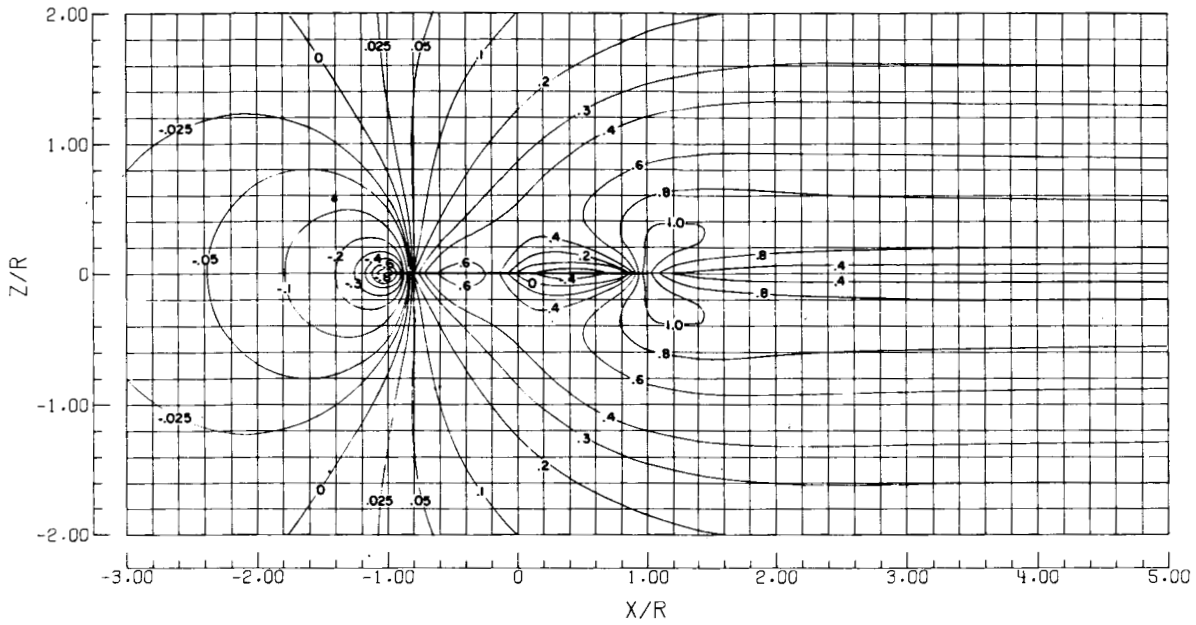
Contours of w/w_0



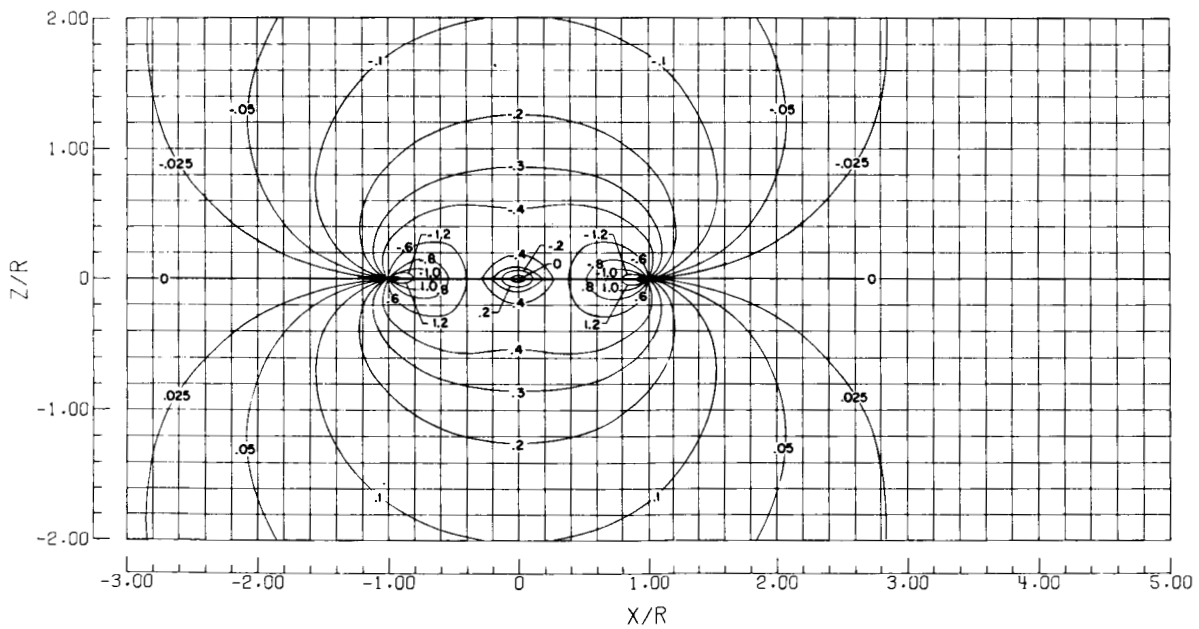
Contours of u/w_0

(b) $\chi = 50^\circ$.

Figure 13.- Continued.



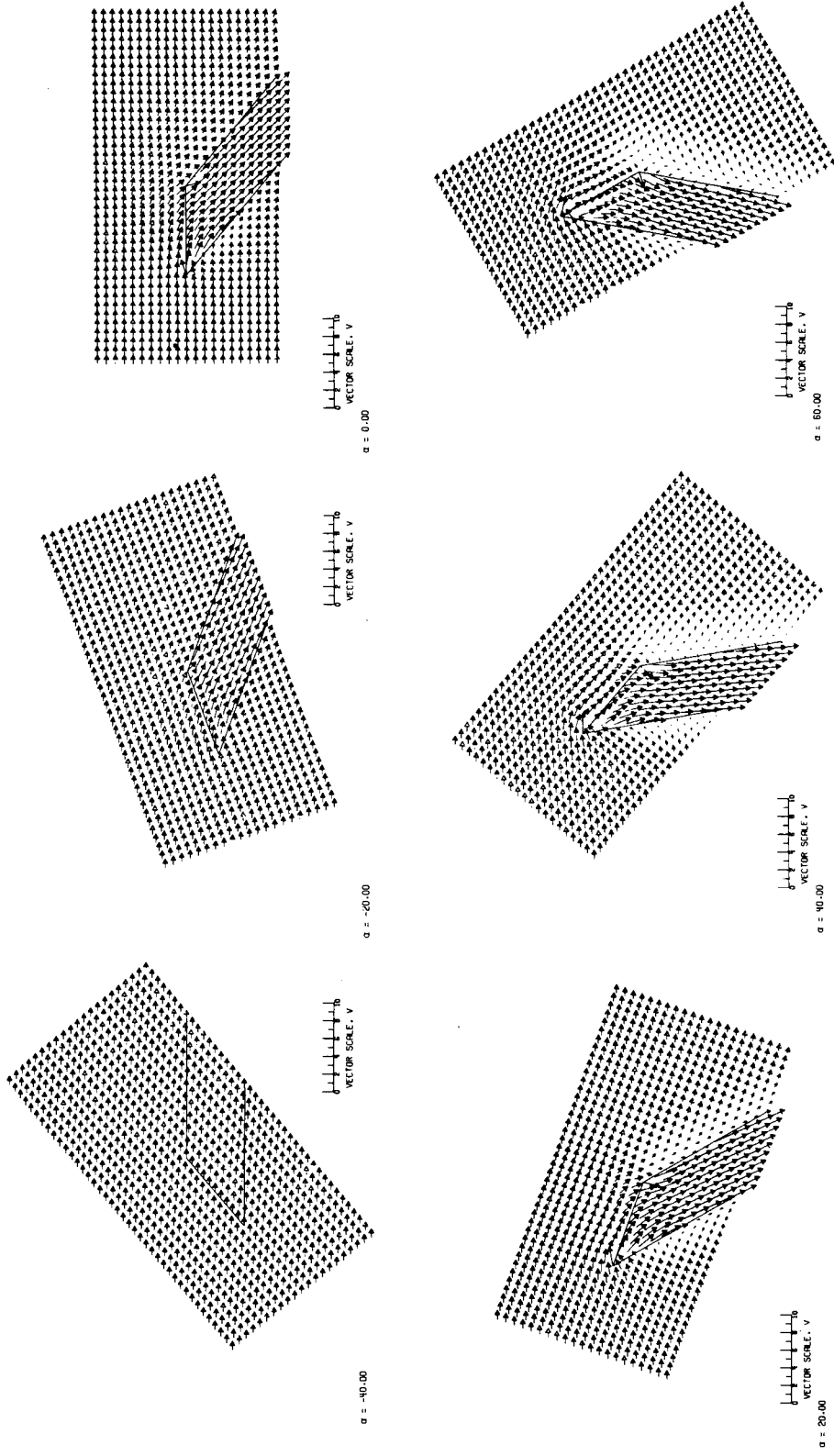
Contours of w/w_0



Contours of u/w_0

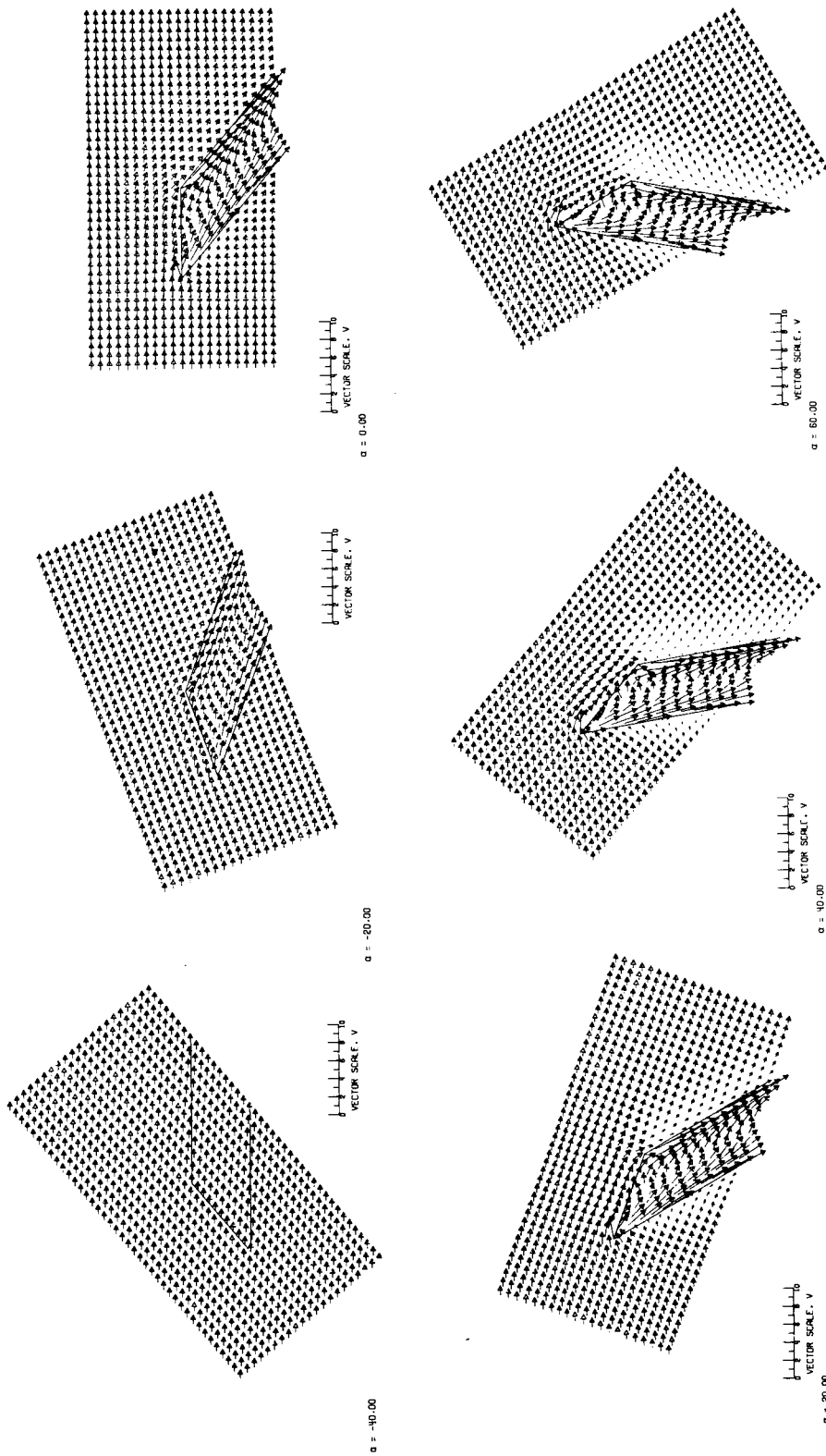
(c) $\chi = 90^\circ$.

Figure 13.- Concluded.



(a) Uniform disk-load distribution.

Figure 14.- Flow field near a rotor with a skew angle of 50° at different angles of attack.



(b) Triangular disk-load distribution.

Figure 14.- Concluded.